High-throughput functionalization of the *Toxoplasma* kinome uncovers a novel regulator of invasion and egress

By

Tyler A. Smith

B.S. Biochemistry, Syracuse University, 2016

Submitted to the Biology Graduate Program in partial fulfillment of the requirements for the degree of

Doctor of Philosophy
at the
MASSACHUSETTS INSTITUTE OF TECHNOLOGY

June 2022

Signature of Author…….
Tyler A. Smith
Biology Graduate Program

Certified by……...
Sebastian Lourido
Assistant Professor of Biology

Accepted by…….
Mary Gehring
Associate Professor of Biology
Member, Whitehead Institute
Co-Director, Biology Graduate Committee

High-throughput functionalization of the *Toxoplasma* kinome uncovers a novel regulator of invasion and egress

By

Tyler A. Smith

Submitted to the Biology Graduate Program on May 16th, 2022, in partial fulfillment of the requirements for the degree of Doctor of Philosophy at the Massachusetts Institute of Technology.

ABSTRACT

Protein kinases regulate fundamental aspects of eukaryotic cell biology, making them attractive chemotherapeutic targets in parasites like *Plasmodium* spp. and *Toxoplasma gondii*. To systematically examine the parasite kinome, we developed a high-throughput tagging (HiT) strategy to endogenously label protein kinases with an auxin-inducible degron and fluorophore. Hundreds of tagging vectors were assembled from synthetic sequences in a single reaction and used to generate pools of mutants to determine localization and function. Examining 1,160 arrayed clones, I assigned 40 protein localizations and associated 15 kinases with distinct defects. The fitness of tagged alleles was also measured by pooled screening, distinguishing delayed from acute phenotypes. A previously unstudied kinase, associated with delayed death, was shown to be a regulator of invasion and egress. I call the kinase Store Potentiating/Activating Regulatory Kinase (SPARK), based on its impact on intracellular Ca^{2+} stores. Despite homology to mammalian PDK1, SPARK lacks a lipid-binding domain, suggesting a rewiring of the pathway in parasites. HiT screening extends genome-wide approaches into complex cellular phenotypes, providing a scalable and versatile platform to dissect parasite biology.

Thesis Supervisor: Sebastian Lourido

Title: Assistant Professor

ACKNOWLEDGEMENTS

I would like to thank the people that have supported me over the years during my doctoral work.

Mr. Tamblin, my high school chemistry teacher, who helped foster my interest in science and taught me to quite literally appreciate the small things. **Coach Myers**, my high school biology teacher and tennis coach, who taught me that no matter how badly you're down to always keep your head up and to focus on the next point.

Dr. Ivan Korendovych who gave me my first research experience by allowing me to join his lab as an undergraduate. **Dr. Caroline Rufo** for being an excellent graduate student mentor and outstanding role model.

Members of my thesis committee – **Dr. Rebecca Lamason** and **Dr. Alan Grossman** – for their scientific insights and advice.

Dr. Sebastian Lourido for your continual mentorship through not only the good experiments and the bad, but a global pandemic. I am grateful for not only your scientific mentorship, but for the opportunity to work in a lab where community and inclusion is deeply valued. Also thanks for letting me decorate your door with artwork.

The Lourido Lab, both past and present. At this point there are too many of you to individually thank. But know that each of you has had an impact on both my scientific and personal development over these six years. I am beyond lucky to work in a lab filled with individuals that are not only so scientifically sharp, but also supportive. Thank you for the insightful science chatter, the coffee breaks, the social hours, and for forcing me to become a runner. Thank you as well for teaching me how to properly pronounce glycerol.

The trainees that I have had the pleasure of mentoring: **Marienela, Gabriella,** and **Sundeep**. Being able to work with each of you has been one of my favorite parts of graduate school. It was truly an honor and a pleasure to have a role in your scientific journeys.

The 2016 Biograds. You were a wonderful and supportive bunch throughout all of my years in graduate school. I can't wait to see what you all go on to do afterwards.

The Snake Slayers and **Explorers without Borders** for many adventures through made-up worlds. Here's to many more.

My teammates on Boop! **Alela**, **Tanners**, and **Tenshi**, you provided a much needed escape from the depths of the pandemic. Of the relatively few good things to come out of the pandemic, your friendship has certainly been one.

Hayden, Dana, Adam, and **Wren**, for many late nights playing video games and decompressing on Discord calls. Thank you for always being an escape from my academia bubble.

Monica Ojeda, for the continual support through all of the trials and tribulations of graduate school and life in general, even though you routinely try to weaponize my low spice-tolerance.

Finally, **my family**. Thank you for always being there for me, whether it be a band concert, musical production, tennis match, or academic endeavor. You have always supported me and graduate school would not have been possible without you.

Thank you to all who have had a role in my graduate school journey. It truly takes a village to raise a graduate student.

TABLE OF CONTENTS

CHAPTER 1: INTRODUCTION

The phylum Apicomplexa

The phylum Apicomlexa constitutes a diverse group of early-branching protists that are obligate intracellular parasites. Members of the phylum Apicomplexa are separated from opisthokonts by over 1 billion years of evolution[1]. To date over 4,000 species have been described[2]. Predictions indicate that this is conservative, with some estimates reaching over 1 million species[3].

Apicomplexans rely on transitions between extracellular and intracellular spaces as well as between defined developmental programs[4–6]. The stages typically include motile, non-replicative extracellular forms and intracellular forms that may be replicative or semi-quiescent. Their dependence on the establishment of an intracellular niche has driven the development of a suite of phylum-specific adaptations that are highly divergent from pathways found in model organisms. The most notable shared characteristic is the apical complex from which the phylum name derives. This complex consists of both secretory organelles and a structural apparatus known as the conoid that facilitates host cell invasion[7]. The apical secretory organelles can be divided into micronemes and rhoptries, which contain contents that are secreted to achieve motility, egress, invasion, and host cell manipulation. The conoid is a tubulin-based complex that serves as a hub for the apical complex and facilitates the docking and organization of the aforementioned secretory organelles[8–10]. The apical complex is conserved across the phylum, consistent with the shared need among apicomplexans to facilitate the extracellular-to-intracellular transitions.

Apicomplexans responsible for human infection include the causative agents of toxoplasmosis (*Toxoplasma gondii*), cryptosporidiosis (*Cryptosporidium* spp.), and malaria (*Plasmodium* spp.). *Cryptosporidium* spp. are one of the most common enteric pathogens and account for up to 12% of childhood diarrheal disease in some regions[11]. The *Plasmodium* spp. represents the most lethal of the human-infecting apicomplexans, with malaria deaths in 2015 estimated to be between 438,000 and 631,000[12]. *T. gondii*,

by comparison, is one of the most widespread pathogens. *T. gondii* parasites can infect virtually any warm-blooded animal, giving the organism a wide range of potential environmental reservoirs[13]. While generally asymptomatic in immunocompetent individuals, it is estimated that *T. gondii* infects approximately a quarter of the global population[14]. Despite their global health burden, many aspects of apicomplexan cell biology remain poorly understood. The genetic tractability and ease of culture within the lab has led *T. gondii* to establish itself as a model apicomplexan with which to elucidate the biology of this global and medically significant phylum.

Toxoplasma disease and life cycle

In humans, the severity of clinical manifestations of *T. gondii* infection are largely dependent on the immunocompetence of their host. Immunocompetent individuals are largely asymptomatic. However, infection of an immunologically naive mother can result in transmission to a developing fetus. Congenital infection can lead to a range of symptoms that are at least partially dependent on the time of infection, some of which include chorioretinitis, blindness, encephalitis, and microcephaly. Immunocompromised patients, such as in the case of Hodgkin's disease or AIDS patients, are at high risk of severe infection. In these cases toxoplasmosis can manifest as encephalitis, pneumonitis, and myocarditis. The symptoms of toxoplasmosis are the result of extensive tissue damage from repetitive cycles of host cell invasion and destruction[14].

Toxoplasma's life cycle is split between a sexual cycle and an asexual cycle. While *T. gondii* can infect all warm-blooded animals, the sexual cycle is restricted to the feline digestive tract[15]. Upon ingestion by a felid host and sexual reproduction within the intestine, highly infectious oocysts are excreted into the environment. These oocysts can persist for months in the environment and are a source of infection via contaminated water or food[15].

The asexual cycle begins with a non-feline and warm-blooded organism ingesting either oocyst-contaminated matter or infected prey. The asexual cycle can occur in virtually any nucleated cell type and is divided into the chronic bradyzoite program and the acute

tachyzoite program. The bradyzoite stage, characterized by slow-replicating parasites surrounded by a cyst wall, is responsible for long-lived latent infections. These cysts are found predominantly in the central nervous system and muscle cells. Current therapeutics are unable to successfully clear encysted bradyzoites from a patient. Consequently, the cysts serve as parasite reservoirs that either revert to the tachyzoite stage in the absence of immune pressure or are transmitted to a new host via predation of cyst-bearing tissues[6]. The tachyzoite stage, in contrast, is characterized by repetitive cycles of host cell entry, intracellular replication, and egress (**Introductory Fig. 1**). Following invasion, the parasites multiply rapidly, doubling roughly every 6–8 hours[16]. The tachyzoite is then able to egress and utilize active motility to invade a neighboring cell. It is these repetitive and destructive tachyzoite cycles that lead to tissue damage and clinical manifestations. The balance between these chronic and acute stages, paired with its broad host tropism, enables *T. gondii* to robustly persist within populations.

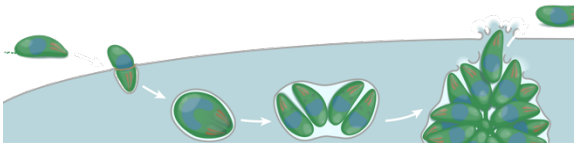

Introductory Figure 1. A schematic of the asexual lytic cycle of *T. gondii* within a host cell.

Toxoplasma lytic cycle

The *T. gondii* lytic cycle begins with invasion of the host cell. This process is dependent on the specialized secretory organelles named micronemes and rhoptries (**Introductory Fig. 2**). Micronemes and rhoptries both reside at the apical end of the parasite, as part of the apical complex[17]. The micronemes secrete components necessary for egress, motility, host cell attachment, and invasion[18–20]. Rhoptry contents are subsequently discharged following host cell attachment. Secreted components from both organelles interact together to form a protein complex known as the moving junction[21–23]. This complex forms a ring around the invading parasite and spans the host-parasite interface. In concert with actomyosin-based motility, the moving junction facilitates entry of the parasite into the host cell and concomitant formation of the parasitophorous vacuole. The parasitophorous vacuole is composed of host cell membrane derived from the point of invasion, however it is depleted of host cell proteins. It has been suggested that the

moving junction forms a molecular sieve that clears the host membrane of proteins and enables the parasite to modify the parasitophorous vacuole with its own secreted contents[24]. The parasitophorous vacuole also evades the endocytic pathway and provides a replicative niche following an active invasion event[25].

Following entry into the host cell, secretion of microneme and rhoptry contents ceases and the secretion of the contents from a third class of secretory organelles, the dense granules, is upregulated[26]. In contrast to micronemes and rhoptries, dense granules are diffusely distributed throughout the parasite and, following host cell entry, are constitutively secreted[17]. Dense granule proteins are responsible for modification of the parasitophorous vacuole. This modification includes the formation of a network of tubular membranes known as the intravacuolar network (IVN). The IVN lies at the interface between the parasite and host cytosol and facilitates export and import between the two[27–31]. The IVN also ensures proper trafficking of nutrients and evasion of the immune response[32–34]. The modification and maturation of the parasitophorous vacuole maintains a stable intracellular replicative niche[35,36].

After establishment of the parasitophorous vacuole, parasites begin replicating via the process of endodyogeny, doubling roughly every 4–6 hours[16]. Through this process two daughter cells are constructed within the mother cell. This replication also is synchronous across all parasites within a vacuole, which share a cytosol via a structure called the residual body[37]. Daughter innermembrane complexes (IMCs), a series of flattened vesicles lying under the plasma membrane (**Introductory Fig. 2**), are constructed within the mother cell. DNA content is doubled and the resulting 2N nucleus is partitioned into each of the two developing daughter cells. As the daughter cells grow, the mother cell is eventually

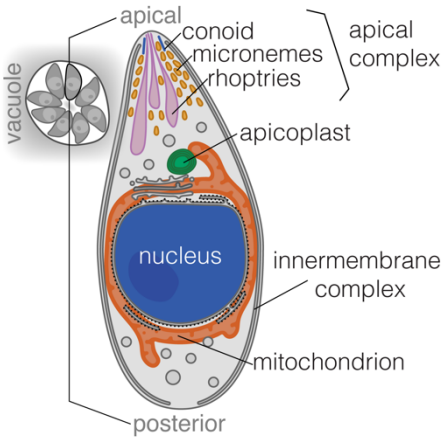

Introductory Figure 2. A schematic of a *T. gondii* cell with the various subcellular structures labeled.

subsumed by the enveloping of the new daughter cell IMC structures with the mother cell's plasma membrane[38].

Approximately 2–3 days post-invasion, at which point the vacuole typically contains between 64 and 128 parasites, the parasites egress from their host cells. The exact trigger of natural egress is unknown, but evidence suggests that it is associated with loss of host cell membrane integrity and accumulation of the lipid phosphatidic acid[39,40]. An increase of parasite intracellular Ca^{2+} triggers both actomyosin-based motility and secretion of microneme contents[6,19,20,41]. The secreted microneme contents include pore-forming proteins necessary for escape from the parasitophorous vacuole and adhesins necessary for host cell attachment and motility. The secretion of microneme contents facilitates egress to complete the lytic cycle and begins the invasion of a neighboring host cell, starting the cycle anew.

The molecular basis of *Toxoplasma* lytic cycle regulation

The molecular mechanisms that regulate the processes of invasion, motility, and egress throughout the lytic cycle have been a focus of the field. These processes are required by all members of the phylum and consequently the associated signaling pathways are largely conserved. While gaps still exist in our understanding, decades of research have identified many of the central genes within this pathway.

As egress from one cell leads into invasion of the next, both processes are preceded by the same signaling cascade (**Introductory Fig. 3**). Intracellular parasites may egress as a result of numerous triggers during the course of natural infection, and the totality of these natural triggers remains unresolved. Intracellular parasites are capable of sensing loss of host cell membrane integrity via a decrease in concentration of host cytoplasmic K^+, although the sensor of this depolarization is unknown[39]. Recent work has also demonstrated that accumulation of phosphatidic acid within the parasitophorous vacuole may serve as a natural trigger for egress[40]. These signals converge on the accumulation of cGMP, produced by the guanylate cyclase (GC), which binds to and activates protein kinase G (PKG)[40,42,43]. Levels of cGMP are determined by the balance

between their rate of production by the guanylate cyclase and their rate of consumption by phosphodiesterases (PDE). Egress can thus be chemically stimulated by treatment with phosphodiesterase inhibitors such as zaprinast or BIPPO, which leads to an accumulation of cGMP and activation of the downstream signaling cascade[44,45]. Conversely, knockdown of the guanylate cyclase and its accessory proteins also inhibits the processes of invasion and egress[40,42,43].

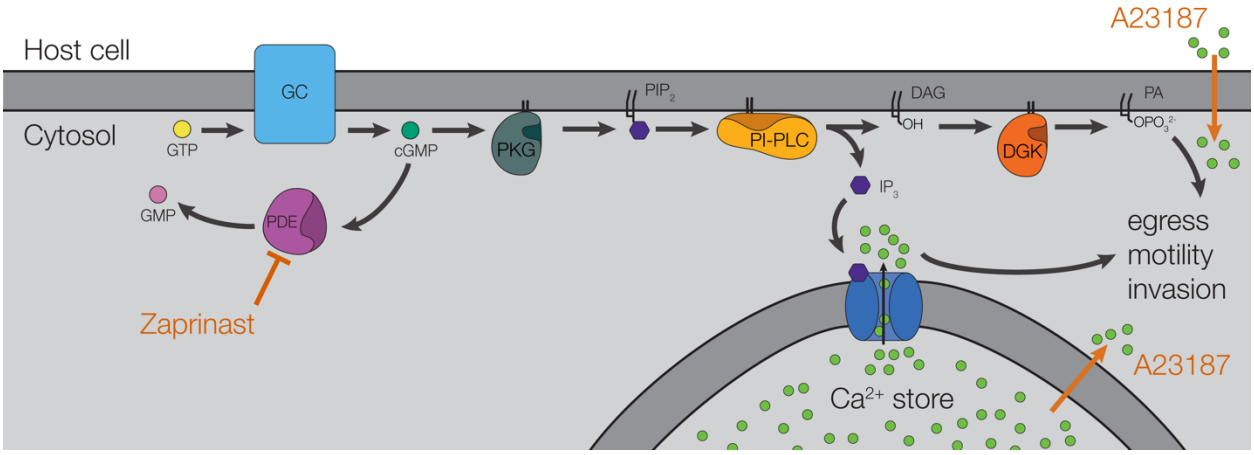

Introductory Figure 3. A schematic of the signaling cascade leading to invasion, motility, and egress. In red are the chemical agonists zaprinast and A23187, which can each stimulate egress via differing mechanisms.

The activity of PKG is essential for microneme secretion, egress, invasion, and motility. Chemical inhibition by the PKG-specific inhibitor Compound 1 or conditional knockdown of PKG completely blocks these processes. Zaprinast-induced egress is likewise blocked by PKG inhibition, consistent with PKG's placement downstream of cGMP production[44,46]. It has also been demonstrated that PKG's localization to the plasma membrane is essential for its function, indicating the importance of spatial regulation of the signaling pathway[46].

It is hypothesized that PKG activity subsequently leads to the cleavage of phosphatidylinositol 4,5-bisphosphate (PIP_2) into inositol 1,4,5-trisphosphate (IP_3) and diacylglycerol (DAG) by the enzyme phosphoinositide phospholipase C (PI-PLC). While direct demonstration of this is lacking, inhibition of PKG in *Plasmodium falciparum* results in a reduction in PIP_2 and an accumulation of its precursors[47]. The mechanism of action of PKG remains unclear, but these results are consistent with its placement

upstream of PI-PLC. In *T. gondii* PI-PLC also localizes to the plasma membrane, placing it spatially close to PKG[48]. Knockdown of the parasite PI-PLC results in abnormal cell division and parasite death, likely due to a disruption of the lipid biosynthetic pathways within the parasite[49].

PI-PLC lies at a split in the signaling pathway, producing both DAG and IP_3. DAG is subsequently phosphorylated by a diacylglycerol kinase (DGK) to produce phosphatidic acid (PA). In support of this model, chemical inhibition of DGKs blocks microneme secretion, invasion, and egress[49]. PA is sensed and linked to microneme secretion by the pleckstrin homology domain of the micronemal surface protein APH, which has been supported by structural studies[49,50].

The second arm of this pathway, IP_3, stimulates release of intracellular Ca^{2+} stores. In other eukaryotes IP_3 directly binds and activates an IP_3 receptor (IP_3R), resulting in release of Ca^{2+} from the endoplasmic reticulum (ER)[51,52]. While no IP_3R has been identified in *T. gondii*, pharmacological evidence supports its existence. Treatment of parasites with ethanol, a stimulant of the IP_3 pathway, leads to an upregulation of IP_3 production, an increase in cytosolic Ca^{2+} levels, and secretion of microneme contents[53]. Addition of IP_3 to isolated *T. gondii* microsomes triggers release of Ca^{2+} and is likewise inhibited by canonical IP_3R inhibitors[54]. Further, work in *Plasmodium falciparum* demonstrated that photolytic uncaging of IP_3 results in a rise of parasite cytosolic Ca^{2+}[55].

The resulting increase in parasite cytosolic Ca^{2+} is both necessary and sufficient to stimulate microneme secretion, motility, and egress of the parasites[19,56]. The sufficiency of Ca^{2+} for these processes in the absence of direct stimulation of upstream production of DAG was demonstrated by treatment with a Ca^{2+} ionophore. This finding indicates the possible presence of a positive feedback loop, although the mechanism of which is currently unexplored. Extracellular Ca^{2+} enhances invasion, motility, and microneme secretion, but intracellular stores alone are sufficient for these processes[56,57]. While the precise source of this intracellular Ca^{2+} is unknown, pharmacological evidence suggests that it lies in a neutral compartment that is also sarco/endoplasmic reticulum calcium ATPase (SERCA)-independent. This suggests that the excitable Ca^{2+} stores lie in either

a sub-compartment of the ER that is depleted of SERCA, or in another organelle entirely[53].

The Ca^{2+} signal is subsequently decoded by a suite of Ca^{2+}-sensitive proteins. The Ca^{2+}-dependent protein kinases (CDPKs) CDPK1 and CDPK3 have both been linked to microneme content secretion, motility, and egress, each to varying degrees[44,58,59]. In addition, CDPK1 is required for invasion[44,59]. The decoding by CDPKs of the IP_3-induced Ca^{2+} signal converges with the DAG arm of the signaling pathway, resulting in the secretion of microneme contents. Among these contents are PLP1, a pore-forming protein required for exit from the parasitophorous vacuole, adhesins that facilitate attachment and motility, and AMA1, a component of the moving junction that tethers the parasite to the host cell during invasion[18,20,21,53,60].

Additional Ca^{2+} sensor proteins include three calmodulin-like proteins, named CAM1, CAM2, and CAM3. Each is important for invasion, egress, and motility, albeit to varying degrees[61]. These proteins co-localize by microscopy and by proximity labeling with myosin H (MyoH) and its light chain MLC7[61]. MyoH and MLC7 are both part of a motor complex that, along with myosin A (MyoA), generates motility via the translocation of adhesins along the parasite axis in an actin-dependent manner[62,63].

Ca^{2+}-sensitive proteins containing C2 domains have also been characterized in *T. gondii*. DOC2.1 bears homology to DOC2 proteins, which in other eukaryotes recruit membrane fusion machinery required for exocytosis[64]. DOC2.1 is required for microneme content secretion in *T. gondii* and *Plasmodium falciparum*, suggesting a similar conserved function among apicomplexans[65]. In contrast, the ferlin protein FER2 is required for rhoptry content secretion and formation of the moving junction, but dispensable for microneme content secretion. While the Ca^{2+}-dependence of FER2 remains to be explored, this represents one of the first pieces of evidence towards Ca^{2+}-dependence in rhoptry secretion[66].

The molecular mechanisms by which microneme and rhoptry membrane fusion and content secretion occur remains an open question. To date, no canonical SNARE

proteins have been characterized in *T. gondii*. Recently, a complex named the rhoptry secretion apparatus (RSA) has been described at the apical tip of the parasites. The RSA is involved in proper docking of the rhoptries and subsequent secretion of their contents, however much of the mechanisms by which this structure operates remain unexplored[67,68].

While the signaling events that orchestrate these processes have been a focus of the field, many mysteries remain, such as the identity of the relevant Ca^{2+} channels and their regulators or the mechanisms of secretory organelle fusion and content secretion. While several relevant protein kinases have been identified, their substrates have yet to be thoroughly explored and validated. The signaling events responsible for leaving the lytic cycle and undergoing the tachyzoite to bradyzoite conversion are even more poorly understood[69]. Cysts remain intracellular, and consequently differentiation needs to be regulated in opposition to rapid replication and egress. While some transcription factors have been linked to the chronic stage transition along with their relevant transcriptomic changes, the consequences of these factors on the downstream signaling network remain largely unstudied[70,71]. Overall, the topology of these signaling networks remains incomplete. Uncovering the molecular basis behind these transitions is critical to our understanding of the life cycle of these ubiquitous parasites.

Eukaryotic protein kinases

Protein kinase structure, enzymatic activity, and substrate recognition

Protein kinases provide important insight into parasite biology as key regulators of cellular processes and are attractive drug targets[72–74]. Through the transfer of the γ-phosphate of ATP or GTP to a serine, threonine, or tyrosine of a target protein, kinases can rapidly alter the structure, and thereby function, of a substrate protein. Analyses of protein kinase domains spanning the eukaryotic kingdom have identified multiple nearly universally conserved features necessary for proper kinase function[75]. The canonical eukaryotic protein kinase domain is approximately 250–300 amino acids in size and consists of a N-lobe and a C-lobe. These lobes are further subdivided into 12

subdomains which each contain highly conserved features and residues responsible for substrate binding and the enzymatic reaction[75].

The lobes of the kinase domain work together to facilitate the transfer of the phosphate group to the substrate protein[75]. Coordination of the nucleotide is also dependent on the presence and formation of a complex with either Mg^{2+} or Mn^{2+} cations. The N-lobe, composed primarily of antiparallel β-sheets and spanning subdomains I–IV, is responsible for coordination of the ATP or GTP nucleotides. In contrast, the C-lobe is largely α-helical, spans subdomains VIA–XI, and is responsible for binding of the peptide substrate[76–79]. Subdomain V spans between the two lobes. It is the cleft between the two lobes that forms the site of catalysis. A lysine in subdomain II orients the nucleotide by coordination to the α- and β-phosphates and is essential for kinase activity. A glutamate from subdomain III is nearly invariant across all protein kinases and helps to stabilize this interaction. A sequence in subdomain VIB known as the "HRD motif" is also critical to enzyme activity. This motif has been termed the catalytic loop because the aspartate serves as a catalytic base for the phosphotransfer reaction. Neighboring asparagine and lysine residues help facilitate this reaction by stabilizing the aspartate residue and the negative charge of the phosphate during transfer. A highly conserved DFG sequence lies in subdomain VII and chelates the activating Mg^{2+} ion and orients the γ-phosphate for transfer. These residues form the core of the ATP/GTP coordination complex and facilitate transfer of the phosphate group to the enzyme's peptide substrate[75].

The broad catalytic cleft of kinases accommodates several residues flanking the substrate phosphorylation site. The variability in these regions contributes to specificity of the phosphorylation site[80,81]. However, kinase recognition motifs are typically only a couple of amino acids in length and are insufficient to restrict the specificity of a given kinase to the observed distinct substrates[82]. Therefore, while the catalytic cleft may determine preferences for a particular site on a given protein, additional interactions are needed in order to achieve stringent substrate peptide specificity between proteins.

These interactions may be in the form of either docking sites present on the kinase that lie outside of the catalytic site, or as tertiary adaptor proteins that bind both the kinase

and the substrate. The AGC kinase 3-phosphoinositide-dependent protein kinase-1 (PDK1), for instance, contains a region known as the PIF-binding pocket. The PIF-binding pocket interacts with a subset of PDK1's potential substrates via an already phosphorylated hydrophobic motif present on the substrate peptides. This is necessary for the recognition and phosphorylation of PDK1 substrates such as S6K and SGK[83]. In the case of protein kinase C (PKC), individual isozymes are associated with specific receptors of activated C-kinase (RACKs). It is the association of specific RACK proteins with each PKC isozyme that determines the substrate specificity, rather than the PKC isozymes themselves[84]. By requiring multiple interaction interfaces kinases are able to achieve stringent substrate specificity.

Protein kinase regulation and localization

The activity of a kinase domain is dependent on its ability to adopt the active kinase fold. Mechanisms of regulation of kinases thereby predominantly rely on transitioning between inactive and active kinase folds. This is reflected by the observation that while the structures of inactive kinase folds vary considerably across kinases, the active forms share topologically very similar catalytic cores[75].

One of the most common mechanisms of kinase activation is by the phosphorylation of a motif known as the T-loop[85]. This loop resides in a variable region that spans subdomains VII and VIII of the kinase domain[75]. Structural studies have demonstrated that phosphorylation of this loop helps stabilize the active kinase conformation[86]. The phosphorylation of the T-loop can occur by either autophosphorylation or by another kinase. PDK1 serves as an activator of other AGC kinases by phosphorylating their T-loop, including the T-loops of other PDK1 molecules[87,88].

Kinases can also be activated via the binding of second messengers or accessory proteins. Binding events can stabilize an active confirmation, relieve an inhibitory binding event, or both. The cyclic nucleotide-dependent kinases protein kinase A (PKA) and protein kinase G (PKG) represent examples of these mechanisms. The catalytic sites are blocked by inhibitory loops originating from either the kinase itself or an associated

regulatory subunit, in the cases of PKG and PKA, respectively. This inhibition is relieved for PKG after a conformational change induced by the binding of cGMP to the regulatory domain[89]. PKA, in contrast, is inactive while bound to its regulatory subunit. Upon binding of cAMP to the regulatory subunit, the catalytic subunit is released and assumes its active conformation[89]. In *T. gondii*, structural studies have established that CDPK1 assumes its active conformation only after the direct binding of Ca^{2+} to its regulatory domain, which relieves autoinhibition and acts as a "molecular splint" for the catalytic domain[90].

Kinase function can also be regulated by localization within the cell. PDK1 was named after its phosphoinositide-binding domain that is present in metazoan orthologs. However, this domain is not essential for *in vitro* kinase activity, which lies in contrast to the aforementioned cyclic nucleotide- and Ca^{2+}-dependent protein kinases. Instead, phosphoinositide binding is important for the co-recruitment of PDK1 and its substrates to the same subcellular location[91]. Similar requirements have been found for some kinases in *T. gondii*. The *T. gondii* ortholog of PKG is acylated and recruited to the plasma membrane. The function of PKG is dependent on this localization. Genetic complementation with strains lacking the acylation motif were unable to rescue knockdown of the endogenous PKG[46].

Despite large amounts of divergence in their signaling networks, apicomplexan kinases operate and are regulated by the same fundamental principles present in the heavily studied kinases of traditional model organisms.

The role of protein kinases in the *Toxoplasma* lytic cycle

The *T. gondii* kinome contains a predicted 108 active kinases and 51 pseudokinases, based on analysis of the kinase subdomains and their conserved catalytic residues[92]. This constitutes approximately 2% of *T. gondii*'s estimated 8,322 protein-coding genes. This proportion is comparable to that of humans (1.7% of the genome)[93]. However, sequence-based functional inference is challenging because evolutionary divergence and parasite-specific adaptations drive the rewiring of signaling pathways. Even broadly

conserved kinase families have acquired dramatic lineage-specific adaptations[94]. Despite these challenges, the roles of a multitude of kinases have been established throughout the parasite lytic cycle as regulators of invasion, motility, egress, replication, and host cell manipulation. In this section I will summarize the kinase classes that have been most heavily studied and linked to the lytic cycle within *T. gondii*. More comprehensive information on the remaining kinases is available in reviews by Peixoto et al. and Gaji et al.[92,95].

The AGC kinases PKA and PKG regulate toxoplasma state transitions

AGC kinases represent a broad family of protein kinases that have been named after the hallmark members protein kinase A, protein kinase G, and protein kinase C. The *T. gondii* kinome contains 10 predicted members of this family[92]. AGC kinases PKG and PKA serve as regulators of the invasion and egress pathways. PKG is necessary for intracellular Ca^{2+} release preceding microneme secretion and is a positive regulator of both invasion and egress[45,96–98]. The *Plasmodium* spp. ortholog of PKG similarly is necessary for Ca^{2+} release and microneme secretion, indicating conservation of this pathway across the phylum.

The *T. gondii* genome contains three annotated PKA catalytic subunits, named PKAc1, PKAc2, and PKAc3[99]. In contrast, there is only a single annotated regulatory subunit, named PKAr. As described previously, PKAc and PKAr form a complex together that, upon the binding of cAMP, dissociates to release an active PKAc subunit[89]. Of note, only the interaction between PKAc1 and PKAr has been established. Knockdown of PKAc1 results in premature egress and repetitive invasion and egress cycles without establishing a replicative niche, indicating that the kinase is a negative regulator of egress[99,100]. This effect was phenocopied by the overexpression of a dominant negative PKAr mutant that was unable to bind cAMP[99].

Intriguingly, PKAc3 is implicated in the transition from the lytic cycle to latency. Knockdown of PKAc3 results in an increase in spontaneous differentiation into the bradyzoite state[101]. These studies indicate that the characterized AGC kinases lie on a

pivotal axis that balances and determines state transitions between invasion, egress, replication, and differentiation.

Ca^{2+}-dependent protein kinases decode intracellular Ca^{2+} fluxes

In other eukaryotes the AGC kinase protein kinase C (PKC) is a primary responder to Ca^{2+} signals. A PKC ortholog has not been identified in apicomplexans, suggesting either a loss of the gene or substantial sequence divergence[94]. Instead, apicomplexans possess an expanded family of Ca^{2+}/calmodulin-dependent protein kinase (CAMK) genes. Contained within this kinase family are the plant Ca^{2+}-dependent protein kinases (CDPKs). Given the absence of CDPKs from metazoan genomes, members of this class have been identified as promising therapeutic targets. These kinases are only activated upon binding to Ca^{2+}[102]. Some of the CDPKs have been linked to the intracellular and extracellular transitions. TgCDPK1 is essential for secretion of the micronemes and consequently invasion and egress[59]. TgCDPK3 in turn is dispensable for invasion but is a regulator of egress[44,58]. The role of the CDPKs as transducers of the Ca^{2+} signals appears to be broadly conserved across the phylum, consistent with the phylum's shared dependence on Ca^{2+} signaling and apical apparatus[103–106].

Rhoptry and WNG kinases facilitate establishment of the intracellular niche

The *Toxoplasma* kinome includes phylum-specific families of secreted kinases that evolved to establish the parasitophorous vacuole niche and to interfere with host cell signaling[92,95,107–111]. The rhoptry kinases are conserved largely across coccidians and reside in and are secreted by the rhoptries during invasion. Rhoptry kinases consist of both active kinases and inactive pseudokinases that contribute to evasion of the immune system across a wide range of host species. This class varies in size across *T. gondii*'s 3 primary lineages (Type I–III), ranging from 37 genes in the Type I strain GT1 to 55 genes in the Type II strain ME49[92]. Variation between strains among the rhoptry kinases is at least partially accountable for differences in virulence[108]. ROP5 and ROP18 were both shown to be responsible for evasion of the murine interferon-gamma response, but were not required for human interferon-gamma evasion[111]. ROP16 is trafficked into the host

cell nucleus where it phosphorylates STAT3 and STAT6, resulting in attenuated response of the IL-12-induced cytokine pathway[112–114].

WNG1 is the founding member of a recently described class of kinases closely related to rhoptry kinases. These kinases were previously annotated as rhoptry kinases, however recent work suggests that they instead localize to the dense granules[107]. These kinases were renamed as WNG kinases after their lack of the conserved glycine-rich loop in the N-lobe of canonical protein kinases (With-No-Gly-loop). Despite its divergence of the conserved glycine-rich region, WNG1 was found to be catalytically active. WNG1 is secreted into the parasitophorous vacuole and is required for the proper formation of the parasitophorous vacuole's membrane ultrastructure[107].

CMGC and aurora kinases are critical for proper cell division

Toxoplasma has also adapted a suite of kinases to regulate its intracellular replication process of endodyogeny, whereby two daughter cells are constructed within and partitioned from a mother cell. Many of these kinases bear homology to mammalian kinases that are responsible for cell cycle regulation, but have been repurposed for *T. gondii*'s unique replicative strategy. Kinases bearing homology to aurora kinases and members of the CMGC family have predominantly been linked to proper cell cycle division and regulation[115–117]. Many apicomplexan kinases seem to have conserved functions in regards to regulation of the cell cycle, but there are key divergences from their mammalian counterparts. Many of the CDK-related kinases (TgCrks) may not be regulated by cyclin partners[115]. Further, the cyclin genes that have been identified in the *T. gondii* genome largely show constitutive expression, as opposed to the canonical cyclical regulation[115,118]. Other CMGC kinases, such as the non-canonical TgERK7, have been adapted for apicomplexan-specific processes such as the proper assembly of the apical complex[9,10].

Despite many annotated protein kinases having mammalian orthologs, it is clear that evolutionary pressures have repeatedly driven the rewiring of these signaling pathways to accommodate the unique state transitions that are demanded by the apicomplexan

life cycles. These transitions maintain a critical balance between fast-replicating acute and persistent chronic stages. The aforementioned studies have substantially progressed our view of the signaling events that regulate apicomplexan life cycle transitions. However, many questions remain unanswered in regards to the kinome of *T. gondii*[92]. For example, despite *T. gondii* possessing 10 predicted AGC kinases, only three (PKG, PKAc1, and PKAc3) have been characterized in detail. While many studies have explored the function of kinases in isolation, systematic and high-throughput approaches can achieve a global view of the contributions of individual enzymes to parasite biology. The development of high-throughput screening approaches in apicomplexans enables rapid analysis of entire gene sets.

Genetic manipulation of *Toxoplasma*

Genome engineering approaches

High rates of transfection, a continuous culture system, and a GC-balanced genome make *T. gondii* parasites attractive model apicomplexans for the use of genetic manipulation techniques. The first genetic manipulations of *T. gondii* parasites utilized the chemical mutagen *N*-methyl-*N′*-nitro-*N*-nitrosoguanidine to introduce point mutations within the genome. Following mutagenesis, temperature-sensitive mutants could be selected and cloned by limiting dilution[119]. This chemical mutagenesis approach was also utilized to isolate mutants resistant to the growth inhibiting nucleosides adenine arabinoside and 5-fluorodeoxyuridine[120,121]. These phenotypes were subsequently mapped to specific genomic loci by performing genetic crosses within cats[122]. The ability to perform genetic crosses, albeit expensive and laborious, was a powerful initial tool that enabled the characterization of complex pathways and the identification of key virulence factors[123–125].

Transfection of *T. gondii* was first reported in 1993 and provided the additional capability to use drug-selectable markers[126–128]. Stable expression of a cassette can be achieved via either random integration into the genome via non-homologous end joining (NHEJ) or homologous recombination (HR). Homologous recombination relies on the presence

of homologous sequences between the transfected construct and a genomic loci. The generation of strains deficient in NHEJ were produced by knocking out the gene *KU80*. These NHEJ-deficient strains suppressed the random integration of transfected constructs and increased the success rate of targeted HR-mediated integration, greatly expediting the process of targeted gene knockout and tagging[129,130].

The most recent advance in *T. gondii* genome engineering has been the adaptation of CRISPR/Cas9 technology to the organism[131,132]. By co-transfecting a Cas9-expression cassette alongside a gRNA-expression cassette, a double-stranded break can be induced at a specific locus, provided it contains an NGG PAM sequence. This double-stranded break is typically repaired by NHEJ and often results in the incorporation of indels and consequently premature stop codons. This generates a functional knockout of the targeted gene. Transfecting two gRNA-expression constructs that target separate locations can result in the deletion of an entire gene segment. Alternatively, the double-stranded break can be repaired by HR, and the aforementioned NHEJ-deficient strains must repair double-stranded breaks primarily through this pathway. Highly efficient gene tagging can be achieved by providing a repair template that encodes the desired epitope tag flanked by sequences that are homologous to either side of the double-stranded break and that are as short as 30 bp[131,132].

Conditional regulation systems

Efficient genome engineering methods also provide the ability to introduce regulatable elements to genomic loci. Precise regulation of *T. gondii* gene expression has been achieved through several methods. Inducible transcriptional control of target genes can be mediated by heterologous promoters[62,133,134]. However, replacement of the native promoter can drastically affect expression levels of the endogenous locus. Alternatively, conditional recombination is possible using a rapamycin-dimerizable Cre recombinase (DiCre). The addition of rapamycin induces the excision of genomic loci that are flanked by short 34 bp sequences called loxP sites. Replacement of a native genomic loci with a gene expression cassette flanked by loxP sites results in inducible control over the locus's expression[135]. An extension of this technology combines C-terminal tagging of a

gene of interest with DiCre-dependent placement of tandem U1-recognition sites at the 3′ end of a gene's coding sequence. Upon induction, the placement of the U1-recognition sites results in efficient gene knockdown[136]. This allows for almost the entirety of the endogenous locus to remain unaltered, with the exception of the 3′ untranslated region. A major drawback of these approaches is that the effects of transcriptional regulation or recombination may be delayed for several replication cycles[135–137].

By contrast, the auxin-inducible degron (AID) system confers post-translational regulation, often achieving knockdown of a target protein within one hour[46,61,138]. In this approach, first adapted from a plant-specific signaling system, a protein of interest (POI) is tagged with an AID in a cell background that also expresses the plant auxin receptor named transport inhibitor response 1 (TIR1). TIR1, while lacking in *T. gondii* and other eukaryotes, is capable of complexing with active SCF E3 ubiquitin ligases. Upon addition of the small auxin molecule 3-indoleacetic acid (IAA), the AID-tagged POI is targeted for ubiquitin-dependent proteasomal degradation[138]. The AID system has been successfully adapted to *T. gondii* and achieves rapid conditional depletion[46,61]. The AID system is also reversible, retains the target gene's native promoter, and can be paired with a fluorescent-protein tag. Deploying the AID system at scale could provide both subcellular localization and temporal resolution to the functional dissection of target genes.

High-throughput screening approaches in parasites

High-throughput screening approaches are powerful tools for the identification of the genes relevant to a wide variety of biological processes. Chemical mutagenesis screens in *T. gondii* generated several temperature-sensitive mutants that exhibited defects across the lytic cycle. Genomic loci responsible for the defects were identified by either complementation with a cosmid library or whole genome mutational profiling[65,139]. This approach however is limited by the ability of individual genes to tolerate the generation of temperature sensitive alleles. Deconvolution of the mutants and assignment of the causative mutation is also exceedingly time-consuming.

Recent high-throughput knockout screens in *T. gondii* and *Plasmodium* spp. have assessed the impact of gene loss on parasite growth[140–145]. CRISPR/Cas9 screening in *T. gondii* has profiled the entire parasite genome for general fitness defects in cell culture and for drug sensitivity[140,145]. Screens targeting smaller gene sets have identified factors linked to bradyzoite formation and virulence within mice[70,143,144]. These screens rely on the induction of a double-stranded break within a gene body and subsequent insertion of the gRNA vector into the genome. This both disrupts the gene body and provides a molecular barcode. After transfecting a library of gRNA vectors into Cas9-expressing parasites and selecting for vector integration, the relative abundances over time of gRNAs within the population can be monitored by next-generation sequencing (NGS). The increase or decrease in gRNA abundances for a given gene serves as a readout of the targeted gene's associated fitness cost.

Screens in *Plasmodium* spp. generated gene knockouts using either homologous recombination (HR) cassettes targeting gene bodies or pseudo-random insertion of a PiggyBAC transposon throughout the genome[141,142]. In *Plasmodium berghei* 2,578 genes (>50% of the genome) were profiled by transfecting 58 separate pools of approximately 100 selectable HR cassettes each into parasites. Each vector targeted a unique gene body and included a molecular barcode whose abundance could be monitored by NGS. Transfected parasites were used to infect mice and the relative fitness cost of each gene was monitored over time by sampling and sequencing vector abundance within mouse blood samples[141].

In *Plasmodium falciparum* transposon mutagenesis by the PiggyBAC transposon was used to profile the genome[142]. The PiggyBAC transposon preferentially inserts at the nucleotide sequence TTAA. The *Plasmodium falciparum* genome has a highly skewed nucleotide composition with >80% AT content and is thus very amenable to the PiggyBAC system[146]. Insertion sites were identified with a NGS technique called quantitative insertion-site sequencing. This approach reached saturating levels of mutagenesis and profiled >95% of the gene for associated fitness costs[142].

High-throughput gene disruption approaches can profile thousands of genes in a single experiment. However, detailed functional characterization and temporal control remain critical challenges. High rates of HR in yeast have enabled the generation of arrayed strain collections for the analysis of protein localization and interacting partners[147–149]. Similar efforts have been undertaken in mammalian cells and the parasite *Trypansoma brucei*; however, no such approach has been implemented in apicomplexans[150–152]. Stable NHEJ-deficient strains, high rates of transfection, and the adaptation of CRISPR-based genome engineering make *T. gondii* ideal for the development of high-throughput tagging methods.

In this thesis I present a high-throughput tagging (HiT) strategy amenable to both arrayed and pooled screening in *T. gondii*. I profiled the kinome of *T. gondii*, assessing subcellular localization and defects in cell division and the broader lytic cycle. Utilizing arrayed screening I assigned localizations to 40 proteins and associated 15 kinases with distinct morphological defects. Pooled screening further distinguished between both acute loss and delayed loss of parasites from a population following gene knockdown. This system provided spatiotemporal resolution that led to the discovery of regulators of various steps in the lytic cycle, including invasion, cell division, and egress. I focused on further characterizing a previously unstudied kinase critical for invasion and egress from host cells, which I name store-potentiating/activating regulatory kinase (SPARK) after its role in the regulation of intracellular Ca^{2+} stores. SPARK is conserved across the phylum Apicomplexa and provides a novel molecular handle with which to further elucidate the architecture of the associated signaling pathways. This system will be a powerful tool to systematically dissect apicomplexan biology.

CHAPTER 2: HIGH-THROUGHPUT FUNCTIONALIZATION OF THE TOXOPLASMA GONDII KINOME

Tyler A. Smith[1,2], Gabriella S. Lopez-Perez[2], Alice L. Herneisen[1,2], Emily Shortt[1], Sebastian Lourido[1,2]

[1] Whitehead Institute for Biomedical Research, Cambridge, MA 02142, USA

[2] Department of Biology, Massachusetts Institute of Technology, Cambridge, MA 02139, USA

The following chapter is adapted from an article published in *Nature Microbiology* (Smith et al., 2022).

Development of high-throughput tagging vectors for *T. gondii*

Pooled knockout screening fails to capture protein localization, expression levels, and the timing of phenotype development. To that end, we developed a high-throughput tagging (HiT) strategy that uses CRISPR-directed homologous-recombination to site-specifically integrate exogenous sequences (payloads), such as epitope tags or regulatable elements (**Fig. 1a**). This strategy is scalable based on cloning from entirely synthetic sequences, a modular design, and the flexibility to construct multiple vectors in a pooled format. HiT vectors encode a gRNA and 40-bp homology regions specific to a target site. HR-mediated repair integrates the synthetic construct into the genome, eliminating the gRNA target site. The integrated gRNA sequence provides a molecular barcode to identify each mutant, making it compatible with both pooled and arrayed screening.

To optimize the HiT system for screening, we designed vectors to tag genes with the mNeonGreen (mNG) fluorophore fused to a minimal auxin-inducible degron (mAID). In *T. gondii* strains containing the heterologous F-box protein TIR1, addition of the auxin indole-3-acetic acid (IAA) leads to proteasomal degradation of the mAID-tagged protein[46,138,153,154]. As test cases, we targeted the kinases CDPK1 and CDPK3, which tolerate C-terminal tags[44,58,59]. We also constructed scarless clones in which the tag was integrated in the absence of additional exogenous sequences, to calibrate the

expression of genes tagged with our HiT vectors. Tagging vectors were co-transfected with a Cas9-expression plasmid. After selection, populations were predominantly mNG positive (**Fig. 1b; Supplementary Fig. 1a**). However, HiT-tagged populations were half as fluorescent as their scarless counterparts. Replacing the *SAG1* 3′ UTR (3′$_{SAG1}$) with the *CDPK3* 3′ UTR (3′$_{CDPK3}$) recovered the expression of the HiT-tagged alleles to near wild-type levels (**Fig. 1b**; bottom row). The correct localizations and UTR-dependent changes in expression were also apparent by live-cell microscopy (**Extended Data Fig. 1a**)[58,59]. Sequencing the gene-tag junctions of isolated clones confirmed correct integration in all the mNG-positive clones (**Fig. 1c**). Nearly all of the selected parasites integrated the HiT vectors in the correct locus, with most harboring the tag in frame—51% of those generated with 3′$_{SAG1}$ and 90% of those generated with 3′$_{CDPK3}$.

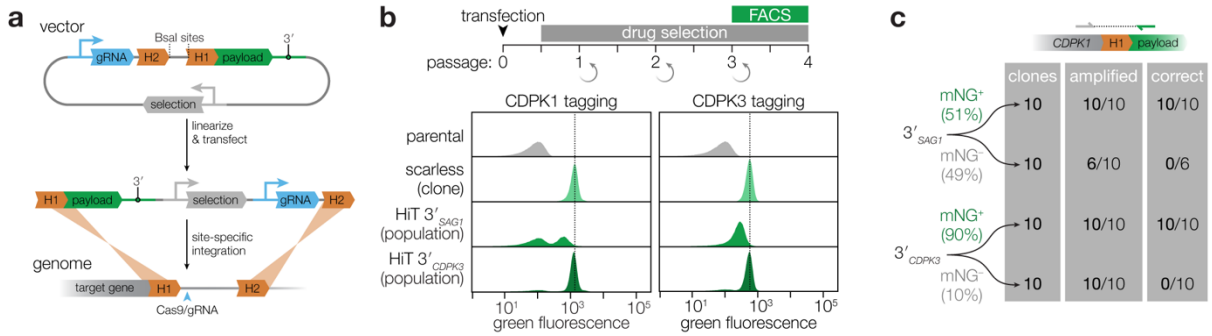

Figure 1. Development of high-efficiency tagging (HiT) constructs for protein-centered screening approaches. a, Schematic of the high-throughput tagging (HiT) vector. The BsaI-linearized vector is cotransfected with a Cas9-expression plasmid into parasites to mediate homologous recombination of the construct into the target locus. H1 and H2 indicate 40-bp regions of homology to the target locus. Pyrimethamine selection was used to isolate integration events. A heterologous 3′ UTR is included in the vector following the tagging payload. **b**, Efficiency of HiT vector tagging. Parental TIR1 parasites were transfected with HiT 3′$_{SAG1}$ or HiT 3′$_{CDPK3}$ vectors targeting *CDPK1* or *CDPK3* with a tagging payload encoding mNeonGreen fused to the minimal auxin-induced degron (mAID). Following selection, the populations were analyzed by flow cytometry and compared to clonal strains carrying the same tag with no exogenous sequences (scarless insertion). Dotted line centered on the mode for the fluorescence of the scarless insertion. **c**, The 5′ integration junctions of 10 mNG positive and 10 mNG negative clones from the CDPK1 HiT 3′$_{SAG1}$ and HiT 3′$_{CDPK3}$ populations were amplified and sequenced. Junctions were categorized according to whether they could be amplified and exhibited the correct sequence at the recombination site.

To demonstrate the versatility of the HiT vector platform, I generated additional vectors targeting CDPK1. I tagged CDPK1 with a V5 epitope linked to the mKate2 fluorophore via a T2A skip peptide (**Fig. 2a**). This HiT vector exhibited highly efficient tagging (**Fig.**

2b–d; **Extended Data Fig. 1b; Supplementary Fig. 1b–c**), and may be used to select for mutants that incorporate the construct in-frame while avoiding the effect of bulky tags. We also generated a HiT vector for transcriptional regulation, using the U1 system (**Fig. 2e**)[137], which conferred inducible knockdown of CDPK1 (**Fig. 2f–g; Extended Data Fig. 1c**). Finally, we confirmed the IAA-induced depletion of our previously used mNG-mAID construct (**Fig. 2h**) and observed complete knockdown (**Fig. 2i–j; Extended Data Fig. 1d**). The AID system is restricted to downregulation of proteins with cytosolic termini; however, the speed of degradation and compatibility with native regulatory sequences makes it the ideal method to target the parasite kinome[46,61,138,155].

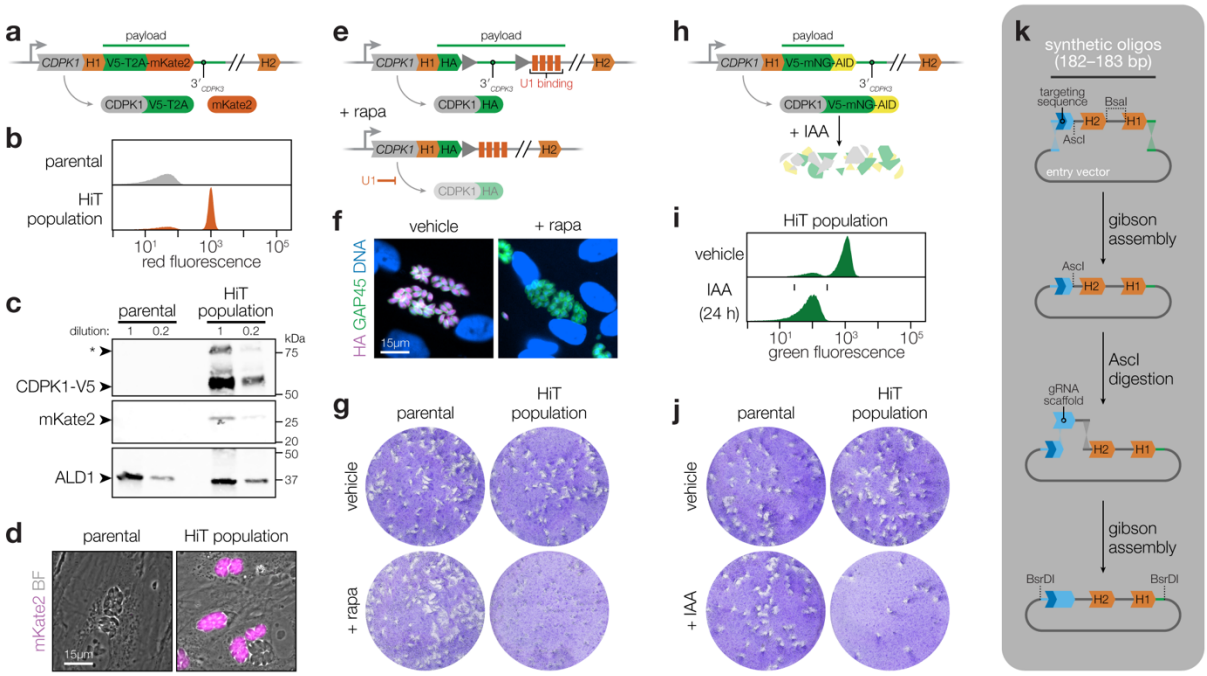

Figure 2. Validation of multiple HiT constructs for protein-centered screening approaches. a, Schematic of *CDPK1* tagged with the V5-T2A-mKate2 HiT vector. **b**, Flow cytometry for mKate2 fluorescence following CDPK1 tagging with the V5-T2A-mKate2 HiT vector and selection. **c**, Immunoblot of the CDPK1-V5-T2A-mKate2 population. Expected MW for CDPK1-V5-T2A and mKate2 are 62 kDa and 26 kDa, respectively. Asterisk denotes full-length protein due to incomplete skipping. **d**, Live-cell microscopy of the CDPK1-V5-T2A-mKate2 HiT population. **e**, Schematic of *CDPK1* tagged with the HA-U1 HiT vector. **f**, Immunofluorescence assay demonstrating CDPK1 depletion following rapamycin (rapa) treatment. **g**, Plaque formation following treatment with vehicle or rapamycin for the parental strain or HA-U1 HiT population. **h**, Schematic of *CDPK1* tagged with the V5-mNG-mAID HiT vector. **i**, Flow cytometry of transfected populations treated with IAA or vehicle for 24 hours. **j**, Plaque formation following treatment with vehicle or IAA for the parental strain or V5-mNG-mAID HiT population. **k**, Pooled construction of libraries with linked gRNAs and homology regions.

Generation of an array of conditional mutants

Protein kinases localize to distinct subcellular compartments to control diverse cellular functions[95]. I designed HiT constructs against 147 protein kinases and 8 control genes, which included genes associated with key lytic cycle transitions, genes previously tagged with the AID system, and a dispensable gene (**Supplementary Table 1**)[49,65,99,100,140,155]. I excluded kinases with predicted signal peptides, based on the expectation that they are inaccessible to the cytosolic TIR1 and largely dispensable in cell culture[140]. I designated 40-bp homology regions upstream and downstream from the cut site, which were paired with three different gRNAs per gene, resulting in 465 unique constructs. Homology region 1 (H1) leads into the tag and includes the 40 bp upstream of the stop codon, while homology region 2 (H2) starts 6 bp downstream of the cut site to prevent futile cycles of cutting.

Since the screens were performed in parallel to the analysis of UTR function, I generated libraries with both *SAG1* and *CDPK3* 3′ UTRs. Short oligos encoding the gRNA and matched homology regions were synthesized and cloned into an entry vector (**Fig. 2k**). The library was linearized to introduce the gRNA scaffold, and then cloned as a unit into the HiT vector to generate the final libraries (**Fig. 3a**). The strategy maintains library diversity while generating thousands of tagging vectors in a single reaction.

I carried out arrayed and pooled screens using the constructed libraries (**Fig. 3a**). Pooled screening is highly scalable, whereas arrayed screening can be used to determine phenotypes through replica-plating and microscopy. To generate the clonal array, the $3'_{CDPK3}$ library was transfected into parasites expressing TIR1[46,61,138,155] and a red-fluorescent inner membrane complex marker (IMC1-tdTomato) to visualize the parasite ultrastructure across the replicative cycle[156]. Following transfection and selection, the population was subcloned by limiting dilution. 1,160 clonal strains were arrayed and passaged in 96-well plates (**Extended Data Fig. 2a**).

I employed dual-indexing PCR to sequence the gRNAs from all 1,160 clonal lines in a single next-generation sequencing experiment. I was able to amplify and assign gRNA

identities to 917 wells, with 87% (796) of the amplified wells containing a single gRNA representing 49% (228) of gRNAs in the original library and 82% (127) of the targeted genes (**Extended Data Fig. 2b**). 121 of the amplified wells contained two or more gRNAs. Only singly tagged clones were used for phenotype and localization studies.

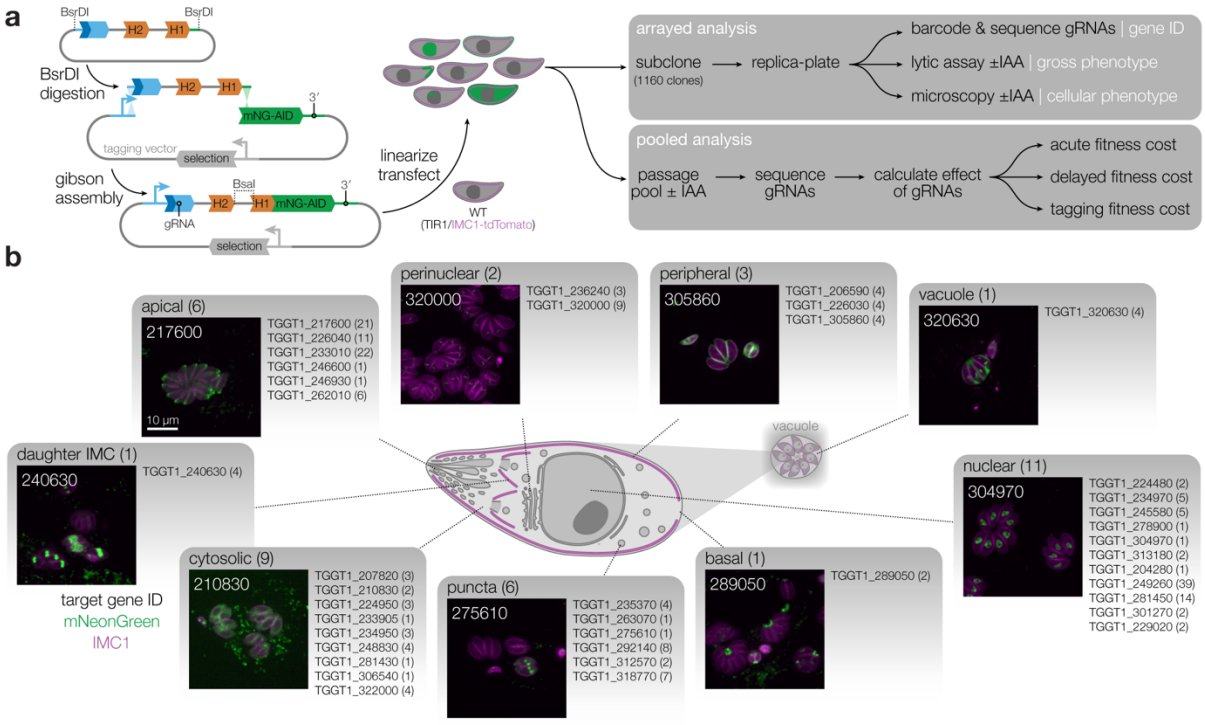

Figure 3. Deconvolution of protein localizations through high-content imaging of arrayed HiT clones. a, Construction of the V5-mNG-mAID HiT vector library and subsequent screening strategy. Following construction and linearization of the library, the vector was co-transfected with a Cas9 expression plasmid into parasites expressing the TIR1 ligase and a fluorescent peripheral marker (TIR1/IMC1-tdTomato). Following selection, the population was analyzed by both pooled and arrayed screening. **b**, Distribution of subcellular localizations for tagged proteins in the array; number of proteins found in each compartment and clones analyzed for each gene indicated in parentheses. Localizations were assigned to a gene if at least half of the uniquely tagged wells for that gene displayed consistent localizations. Representative confocal images of sample clones are displayed with genes numbered based on their unique identifier (e.g., TGGT1_210830, labeled 210830). Images are maximum intensity z-projections for mNeonGreen (green) and IMC1-tdTomato (magenta).

Localizations and phenotypes of tagged proteins in the arrays

I employed high-content imaging to visualize the localization and IAA-induced depletion of tagged proteins, and monitor the consequences of their knockdown. Arrayed clones

were replica-plated, treated with IAA or vehicle 3 h post-infection, and imaged the following day. 232 (29%) clones displayed a clear mNG signal, enabling unambiguous localization of 40 proteins to diverse subcellular compartments (**Fig. 3b**; **Extended Data Fig. 3–4**; **Supplementary Table 2**). Some proteins, such as TGGT1_275610, consistently displayed heterogeneous expression, likely indicating cell cycle regulation. 36 of the 40 proteins localized showed complete depletion after 24 h of IAA treatment. TGGT1_226040, TGGT1_322000, TGGT1_320630, and TGGT1_234950 showed minimal signal reduction under IAA. Localization to the parasitophorous vacuole (TGGT1_320630) or dense granules (TGGT1_234950)[157], suggests inaccessibility to TIR1 may account for the lack of degradation. Nevertheless, HiT screening can generally localize parasite proteins with high-throughput.

Knockdown-induced phenotypes were classified based on parasite structure. Mutants in TGGT1_304970, TGGT1_313180, TGGT1_234970, or TGGT1_245580 arrested early in the lytic cycle (**Fig. 4a**). Degradation of the latter two caused a discontinuity in the IMC marker (singlets II). Accordingly, TGGT1_304970 is a cyclin–related kinase (TgCrk1) required for daughter cell assembly[115] and TGGT1_234970 is a nuclear tyrosine kinase-like protein (TgTKL2)[158] related to the human Tousled-like kinase that promotes DNA replication[159–161]. The two other singlet kinases are also nuclear: TGGT1_313180 is related to a yeast splicing factor[162]; and TGGT1_245580 is large, exclusively found in coccidians, and lacks any other distinguishing features.

The remaining cell division phenotypes could be broadly categorized as exhibiting a continuous (cell division I) or fragmented (cell division II) IMC distribution (**Fig. 4a**). Within these categories, I found two previously described cyclin-related kinases, TGGT1_256070 (TgCrk4) and TGGT1_229020 (TgCrk5). Knockdown of TgCrk4 causes major morphological abnormalities and decreased plaque size[115]. The function of TgCrk5 has not been previously examined, although it was shown to interact with the cell cycle regulator ECR1 at the centrocone[118]—consistent with our observations (**Extended Data Fig. 3a**). Indeed, our knockdown of TgCrk5 mirrored the phenotype of a temperature-sensitive allele of *ECR1*[118]. Knockdown of the centrosome-associated kinases NIMA-

related kinase 1 (TgNek1; TGGT1_292140), MAPK-like protein 1 (TgMAPK-L1; TGGT1_312570), and TgMAPK2 (TGGT1_207820) phenocopied previously characterized conditional mutants[116,139,163,164]. TgMAPK-L1 displayed cell cycle–dependent localization to diffuse puncta, consistent with its localization to the pericentrosomal matrix. In addition to the reported cytosolic localization[164], TgMAPK2 was observed at paired puncta in a subset of vacuoles, shedding additional light into the function of this kinase.

Cell-cycle defects were also observed for several kinases that have not been previously studied. Knockdown of TGGT1_240410 phenocopied TgMAPK-L1 disruption, despite being conserved only among related coccidians. How other kinases regulate the cell cycle is unknown, but they can be associated with cellular functions based on their localization and similarity to well-studied orthologs: TGGT1_235370 and TgMAPK2, TGGT1_224480 and Cdc-like kinases that regulate the mammalian spliceosome[165], and TGGT1_210830 and RIO kinase 1 that participates in ribosomal maturation[166]. As with TGGT1_210830, knockdown of TGGT1_268010 caused an arrest after a single cell cycle, although its conservation is restricted to coccidians. Accumulation of the IMC marker with grossly normal organization resulted from knockdown of TGGT1_278900, for which homology to yeast BUD32 and association of the *Plasmodium falciparum* orthologue with the EKC/KEOPS complex components suggest conservation of the complex across eukaryotes[167].

I also screened for aggregate defects in the lytic cycle by examining monolayer clearance after knockdown (**Fig. 4b**). Changes in monolayer clearance were compared to positive and negative controls. All positive controls and 109 clones (11%) scored three standard deviations above the average lysis inhibition score for the negative controls. The 109 clones represented 21 genes (17% of genes tested), including every mutant identified by high-content imaging except TgMAPK2, which displayed an incompletely penetrant phenotype. By contrast, clones in which ERK7 or Doc2.1 were tagged displayed defective monolayer clearance but no morphological changes by microscopy, consistent with reported roles in invasion and egress but not replication[9,10,65]. TGGT1_306540

shared these phenotypes with ERK7 and Doc2.1, and appears to be a cytosolic ethanolamine kinase (TgEK)[168] necessary for the completion of the lytic cycle. Our results highlight that arrayed HiT screening can capture both localization and detailed cellular phenotypes.

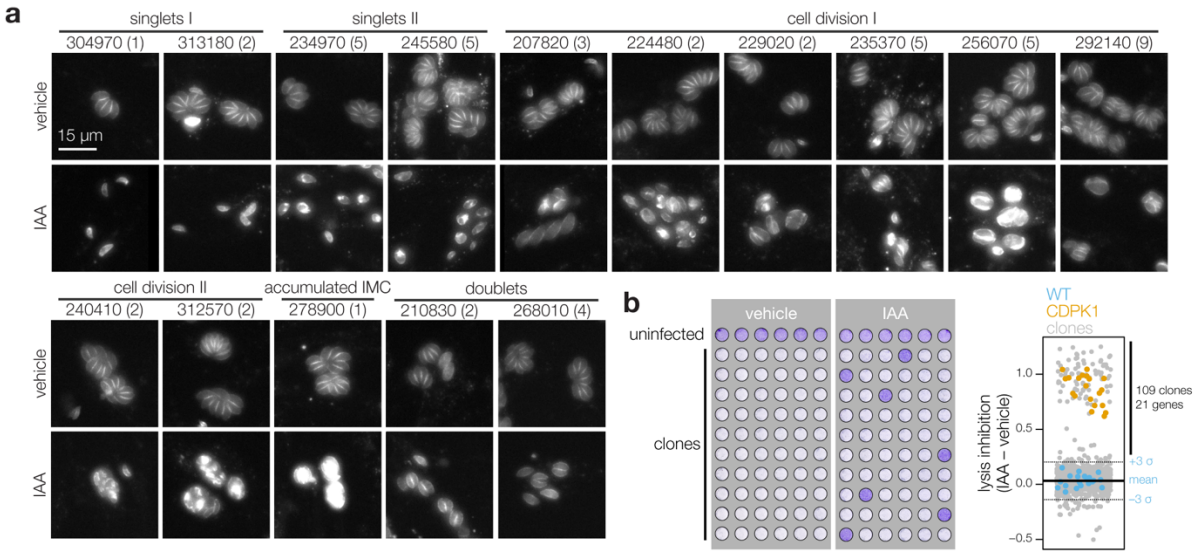

Figure 4. Assignment of protein phenotypes through high-content imaging of arrayed HiT clones. a, Widefield microscopy of representative clones with identified phenotypes. Images are maximum intensity z-projections. The IMC1-tdTomato marker is displayed for cultures treated with either vehicle or IAA for 24 h. Phenotypes were binned into six categories based on their similarity. Number of clones analyzed for each gene indicated in parenthesis. **b**, The ability of clones to lyse fibroblasts was assayed by infecting monolayers for 72 h in the presence or absence of IAA. Intact monolayers were visualized by crystal violet staining. Normalized absorbance measurements comparing vehicle- and IAA-treated wells are graphed for each clone. Each plate contained the parental strain (WT) and an AID-tagged CDPK1 clone (CDPK1) as controls. Mean ± S.D. for WT controls are shown.

Temporal resolution of phenotypes by pooled screening

Pooled screening offers greater scalability and a more sensitive comparison of mutant fitness than arrayed screening. To perform pooled screens, $3'_{SAG1}$ or $3'_{CDPK3}$ HiT vector libraries were transfected into TIR1 or TIR1/IMC1-tdTomato parasites, respectively. After three passages under pyrimethamine selection, the populations were split and treated with vehicle or IAA, collecting samples to quantify gRNA abundances at each passage (**Fig. 5a**). The abundance of gRNAs in the array was strongly correlated to their abundance in the $3'_{CDPK3}$ pool before IAA treatment (**Extended Data Fig. 4e**). The relative

abundance of a given gRNA could be affected by (i) the efficiency of integration, (ii) locus tolerance to tagging, and (iii) the consequence of protein degradation by IAA. As expected, gRNAs targeting sequences with NAG PAMs were less efficiently integrated than those targeting NGG PAMs[169] (**Fig. 5b**). To regress the effect of the PAM, I normalized the abundance for NAG gRNAs at each time point by the difference in mean abundance between NAG and NGG guides for genes considered dispensable[140] within each sample. I calculated the fold change relative to the second passage, when relative gRNA abundances best reflected the composition of subsequent populations, allowing us to merge the results of both screens.

I compared the trajectories for gRNAs across time and IAA treatment. Using UMAP for dimensionality reduction followed by k-means clustering[170,171], the groupings of gRNAs largely agree with previously determined phenotype scores of the target genes (**Fig. 5c–d**)[140]. Notably, cluster 1 was enriched in gRNAs that differentially dropped out of the population following IAA treatment (**Fig. 5e**), suggesting the targeted genes are fitness-conferring and their gene products are successfully depleted upon IAA treatment.

I next calculated the centroid in UMAP space for gRNAs from both screens to measure the performance of individual genes. Unsupervised clustering on the centroids assigned genes to two classifications, one of which, cluster A, included 47 genes and was highly enriched for contributing to parasite fitness (**Fig. 5f**). The arrayed screen captured mainly acute phenotypes and 18 of the 22 genes that had deficits by microscopy or lytic assay were found in cluster A. 13 of the cluster A genes were not represented in the array, and the remaining 16 likely display phenotypes difficult to appreciate in isolation or during brief periods of kinase depletion. Discrepancies between the two screens may also result from the analysis of incorrectly integrated vectors in the array; such clones could be theoretically excluded based on lack of tag expression, but that strategy would sacrifice lowly abundant protein kinases. Out-of-frame integration may also be frequent for proteins rendered hypomorphic by the tag and may drive known essential genes like PKG[46,172] into cluster B.

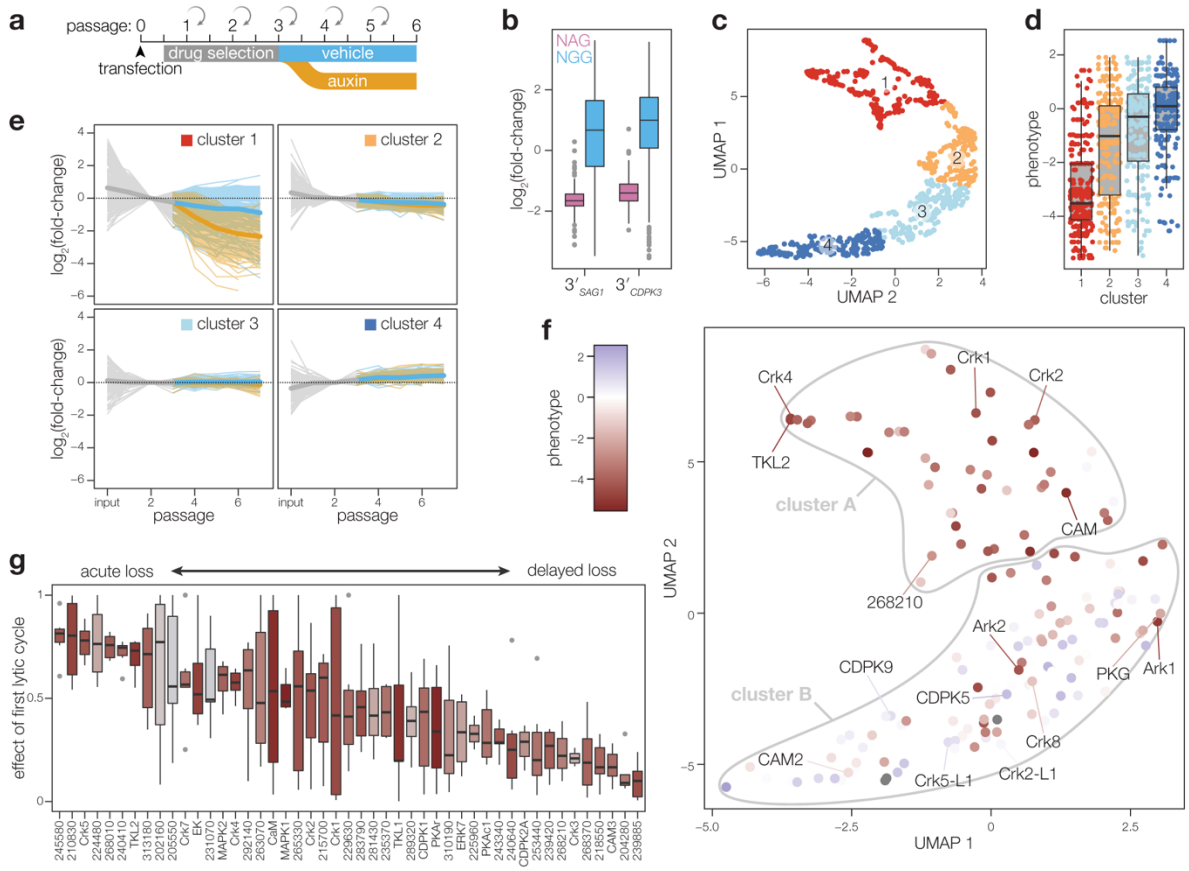

Figure 5. Pooled screening distinguishes between acute and delayed-loss phenotypes. **a**, Schematic of pooled screening workflow. Transfected populations were selected with pyrimethamine for three passages, after which they were split and cultured in either vehicle- or IAA-containing media. Following each lysis, parasites were split to collect samples for next-generation sequencing and continue propagating in fresh host monolayers. **b**, Fold-change in gRNA abundance between the vehicle-treated passage 6 and the initial library, plotted by PAM type. Boxplot displays the distribution of each sample by quartiles; outliers highlighted in gray; *n* = 107 NAG and 358 NGG gRNAs. **c**, Relative abundances for each guide were corrected for the effect of the PAM used and fold-changes were normalized to passage 2. UMAP was used to compare guides in each screen based on their pattern of fold changes for vehicle- and IAA-treated samples. Clusters were calculated by k-means. **d**, Comparison of phenotype scores from prior gene-disruption screen for each of the clusters in **c**. Boxplot displays the distribution of phenotypes in each cluster by quartiles; *n* = 253, 205, 209, 215 gRNAs per cluster. **e**, Pattern of fold changes for each guide plotted by cluster. Lines colored by treatment, as in **a**. Bold lines are the mean for all guides in a given cluster. **f–g**, Gene centroids in UMAP space based on the effects of targeting guides against each gene (**f**). Genes were assigned to fitness-conferring (cluster A) or dispensable (cluster B) categories based on k-means clustering. Fraction of the maximum fold-change that is explained by the first lytic cycle following IAA addition for all fitness-conferring genes in cluster A, ordered based on the magnitude of the effect from acute loss to delayed loss (**g**); *n* = 6 gRNAs per gene. Individual genes colored based on the phenotype scores from the prior gene-disruption screen[12].

Two of the four genes identified by the arrayed screen but not the pooled screen (TGGT1_218720 and TGGT1_250680) likely represent false positives in the arrays, since they were only represented by single clones with modest defects in the lytic assay and were dispensable in previous knockout screens[140]. By contrast, the two other genes missed by the pooled analysis (TGGT1_278900 and TGGT1_240910) are expected to be fitness-conferring[140], and TGGT1_278900 degradation was associated with accumulation of the IMC marker (**Fig. 4a**). Three clones of TGGT1_240910 (Doc2.1; included as a control based on prior studies[65]) displayed the expected lytic assay phenotype upon knockdown. For some genes (e.g., Doc2.1), the discrepancy between screens originated from contradictory results between different gRNAs when the population was treated with IAA; however, we noticed that gRNAs with optimal designs—based on proximity to the coding sequence or use of an NGG PAM—were more likely to conform to expectations.

I next investigated the timing of gRNA loss for genes in cluster A. I sorted genes based on the fraction of the maximum effect from IAA treatment that was observed after a single lytic cycle (**Fig. 5g**). 14 of the 15 genes associated with defects by microscopy (TGGT1_278900 was missed by the pooled screens) dropped out substantially during the first passage in IAA. TGGT1_215700 and TGGT1_270330 (TgCrk7) dropped out acutely but were absent from the array, and the latter is considered essential[115]. TGGT1_215700 is broadly conserved across eukaryotes and homologous to phosphatidylinositol kinases critical for proliferation in other organisms[173,174]. This temporal resolution was not observed in conventional CRISPR-based screens (**Extended Data Fig. 4f**). Our results suggest that this analysis can identify genes whose disruption leads to immediate and catastrophic defects in the parasite.

In contrast to the acute defects associated with some genes, gRNAs against other genes were mostly retained during the first lytic cycle (**Fig. 5g**). Delayed-loss phenotypes were assigned to several genes linked to invasion or egress: CDPK1, ERK7, PKAc1, TKL1, and CAM3[9,10,59,61,99,100,158]. These genes lacked defects during the brief window selected for microscopy. Another delayed-loss gene, CDPK2A, belongs to a kinase family that

has been linked to invasion and egress[44,58,59,103,104,175,176]. TGGT1_249260 (TgCrk3) similarly displayed no defects by microscopy or lytic assay, consistent with the observation that knockdown reduced plaque size but did not impact morphology[115]. Pooled screens more easily capture subtle defects that accrue over several lytic cycles and may involve processes that accompany egress and invasion.

Discussion

HiT screens benefit from both arrayed and pooled formats. Arrayed screens examine individual clones to characterize subcellular localizations and cellular defects, even in cases when they are heterogeneous or incompletely penetrant. Pooled screening, by contrast, compares all targeted genes simultaneously, detecting subtle defects that are only apparent in competitive settings. Arrayed screens for protein localization in *Trypanosoma brucei* successfully localized most gene products[150]. Pooled screens in *T. brucei*, *Plasmodium* spp., and *T. gondii* have examined genetic contributions to fitness, but lack temporal or subcellular resolution[140–143,177]. Arrayed and pooled HiT screens work in tandem to achieve protein localization and phenotypic resolution inaccessible to existing platforms. Further, clonality ensures unambiguous localization, uniform knockdown, and recovery of individual clones from the arrays for follow-up studies.

While false positives in the HiT screens were minimal, 29 genes previously reported to be fitness-conferring[140] were missed. False negatives likely originate from poor-quality gRNAs, inaccessibility of the tagged protein to TIR1, and tagging-induced hypomorphism. Reduced abundance of low-quality gRNAs also caused skewed sampling in the array. Future screens should use more gRNAs per gene, avoid targeting NAG PAMs, and array clones soon after transfection. Alternative HiT payloads can constitute regulatory elements instead of a protein tag—as demonstrated by regulation of CDPK1 with the U1 system (**Fig. 2e**)—achieving regulation of inaccessible proteins or of those rendered hypomorphic by tags.

I identified several previously unstudied regulators of the parasite lytic cycle. Knockdown of each of four nuclear kinases caused early arrests, reminiscent of blocks in G_1 or S/M—

such kinases likely regulate critical checkpoints. By contrast, later arrests may be associated with a restriction of resources. This is supported by the phenotype of TGGT1_210830, the ortholog of which is critical for ribosomal maturation[166]. Other phenotypes included abnormalities in parasite morphology. Multiple genes displayed defects similar to those previously observed for TgMAPK-L1 and TgMAPK2[116,139,163,164]. Aberrant morphologies allude to failures in daughter cell assembly or cytokinesis. The visualization of cellular consequences following gene knockdown expands upon general fitness screening leading to specific hypotheses regarding gene function. The cellular defects observed also reflect acute and lethal consequences for the parasites, establishing these kinases as promising therapeutic targets.

HiT screens expand current platforms and enable the identification of complex cellular phenotypes. This technology can already handle much larger gene sets (~2000 genes) than the kinome. The AID system is reversible[138], which could help distinguish temporary arrests in replication from lethal disruptions. Alternative tags or conditional expression systems, can also extend HiT screening to additional questions and make it compatible with secreted or compartmentalized proteins inaccessible to the AID approach. Concurrently with our work, Jimenez-Ruiz and colleagues developed an alternative strategy for high-throughput phenotypic analysis of *T. gondii*, which implemented a rapamycin-inducible split Cas9 to precisely time gene disruption[178]. Together with the HiT screens, these technologies offer unprecedented spatiotemporal resolution to screening in *T. gondii* and are powerful tools for dissecting the biology of these ubiquitous apicomplexan parasites.

CHAPTER 3: SPARK REGULATES INVASION AND EGRESS

Tyler A. Smith[1,2], Gabriella S. Lopez-Perez[2], Alice L. Herneisen[1,2], Emily Shortt[1], Sebastian Lourido[1,2]

[1] Whitehead Institute for Biomedical Research, Cambridge, MA 02142, USA

[2] Department of Biology, Massachusetts Institute of Technology, Cambridge, MA 02139, USA

The following chapter is adapted from an article published in *Nature Microbiology* (Smith et al., 2022).

Two delayed-loss kinases regulate invasion

I characterized four delayed-loss candidates with patterns of gRNA loss that contrasted with the rapid depletion of representative acute-loss genes (**Fig. 6a**). All four kinases were fitness-conferring in genome-wide knockout screens[140] and remain largely uncharacterized. The four kinases exhibit different phyletic patterns[179]: TGGT1_204280 is conserved among several single-celled parasitic phyla, including kinetoplastids and amoeba; TGGT1_268210 and TGGT1_239420 are restricted to Apicomplexa; and TGGT1_239885 is restricted to coccidians. TGGT1_239420 was previously linked to the development of artemisinin resistance in vitro[180]. Intriguingly, the *Plasmodium falciparum* ortholog of TGGT1_268210 (PfPDK1; Pf3D7_1121900) was classified as fitness-conferring in previous screens and has been linked to the regulation of protein kinase A (PKA)[142,181].

Although three of the candidates were in the array, I rederived conditional mutants to independently validate the screening results. I placed each mutant in competition with TIR1/IMC1-tdTomato parasites under knockdown conditions. A second wildtype strain was used as a control for the assay. All four mutants were outcompeted by wildtype, demonstrating the kinases contribute to parasite fitness (**Fig. 6b; Supplementary Fig. 2**). Three of the mutants also showed clear defects in plaque formation when grown in the presence of IAA (**Fig. 6c**); knockdown of TGGT1_239420 or TGGT1_239885 reduced

plaque size, while knockdown of TGGT1_268210 blocked plaque formation (**Fig. 6d**). The lack of a plaquing defect for TGGT1_204280 suggests a subtle or merely competitive defect in fitness.

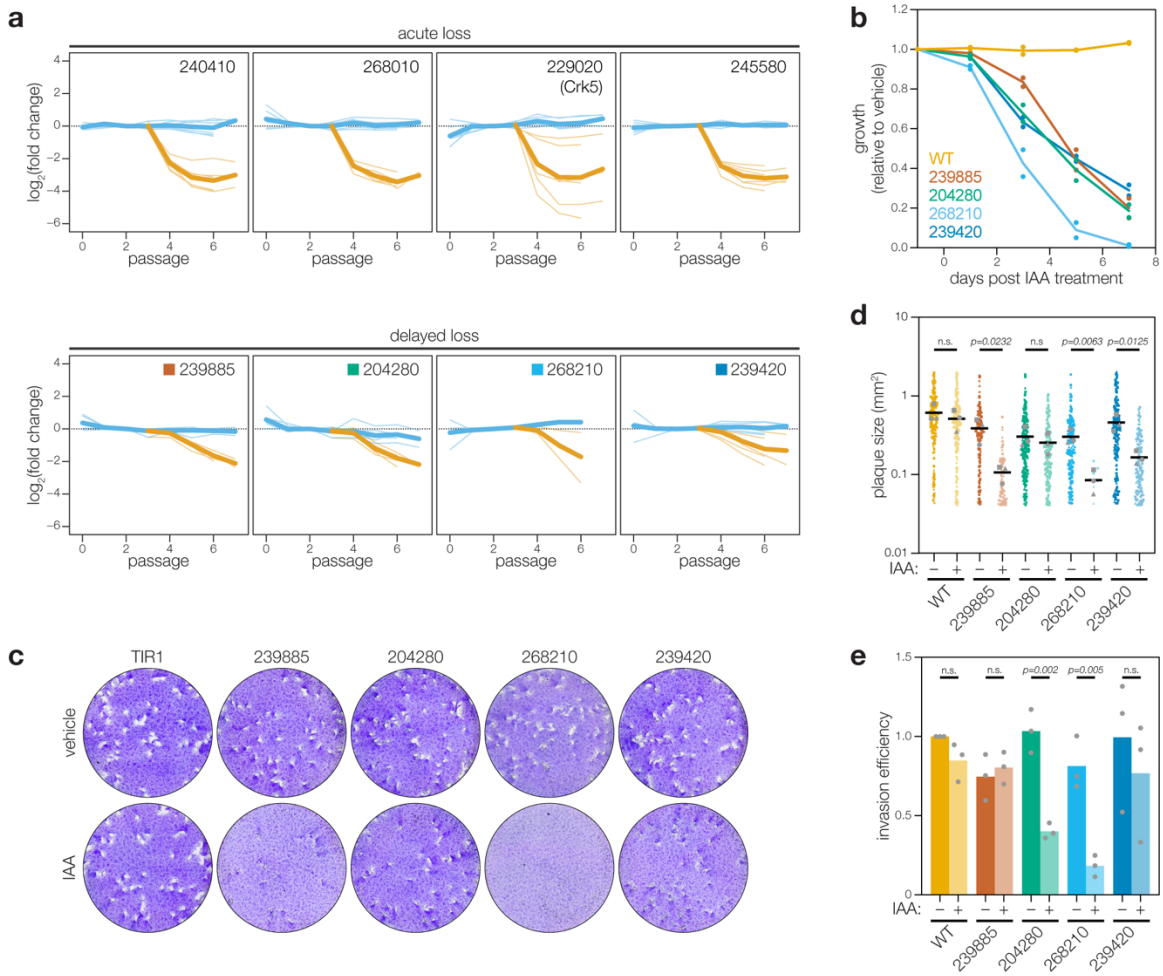

Figure 6. Analysis of delayed-loss genes identifies two kinases that impact invasion. a, Pooled screening traces of selected acute- and delayed-loss genes. The fold change of individual guides in the vehicle- (blue) and IAA- (orange) treated samples are displayed. Bold lines are the mean for all guides in a given condition. **b**, Competition assays of delayed-loss candidates, compared the relative growth of AID-tagged strains against a wild-type strain in either vehicle- or IAA-containing media. Following each lysis, the proportion of fluorescent parasites within each competing population was measured by flow cytometry and normalized to the vehicle control; $n = 2$ biological replicates. **c–d**, Plaque assays of delayed-loss candidates grown in the presence of IAA or vehicle control (**c**). The parental strain (WT) is included for comparison. Quantification of plaque areas from three separate wells are plotted (**d**). Means are displayed; n.s. $p > 0.05$, two-tailed *t*-test. **e**, Invasion assays of delayed loss candidates. AID-tagged strains grown in vehicle- or IAA-containing media for 24 h were incubated on host cells for 10 minutes prior to differential staining of intracellular and extracellular parasites. Parasite numbers were normalized to host cell nuclei for each field. Means graphed for $n = 3$ biological replicates; n.s. $p > 0.05$, Welch's one-tailed *t*-test.

I assayed the invasion efficiency of all four mutants, as a potential cause of the delayed-loss phenotype. Both TGGT1_268210 and TGGT1_204280 displayed significant invasion defects upon knockdown (**Fig. 4e**). Since parasites formed normal plaques upon TGGT1_204280 knockdown, the invasion defect may represent a delay rather than a complete block. By contrast, the severe invasion defect of TGGT1_268210, coupled with effects in plaque formation and competition assays, suggests the gene plays a critical role in the lytic cycle.

SPARK regulates intracellular Ca^{2+} store release

I examined TGGT1_268210 (hereafter referred to as SPARK) in greater detail. SPARK belongs to the AGC kinase family. Despite homology to mammalian PDK1 (**Fig. 7a**), SPARK lacks the canonical C-terminal phosphoinositide-binding domain, similarly to related kinases in yeast and nonvascular plants[182]. Instead, SPARK and its apicomplexan orthologues possess an N-terminal MKXGFL motif absent from canonical PDK1s (**Fig. 7b**). Free-living alveolates *Vitrella brassicaformis* and *Chromera velia* harbor two PDK1-

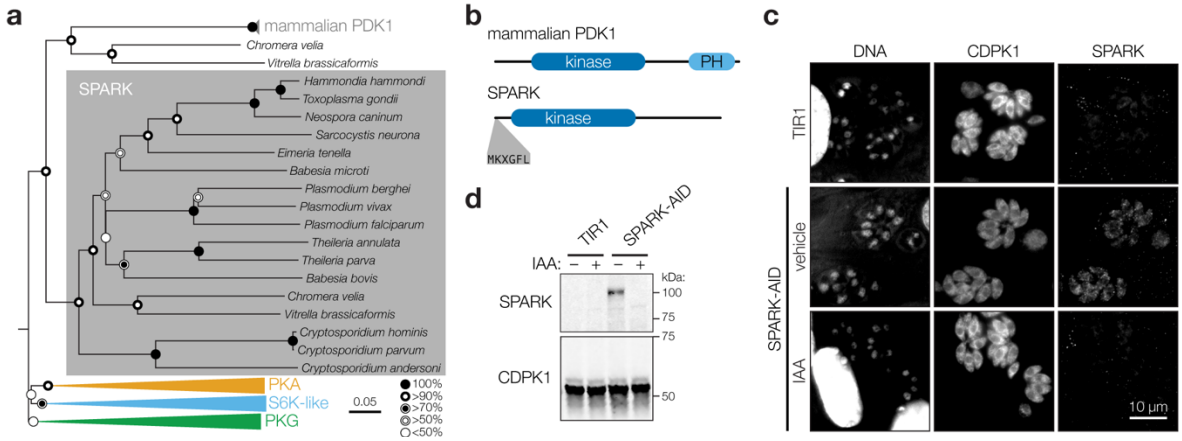

Figure 7. SPARK is a conserved apicomplexan kinase with distant homology to PDK1 kinases. a, Neighbor-joining phylogenetic tree of kinase domains from representative apicomplexan species, along with mammalian PDK1 orthologues and related AGC kinases. Bootstraps determined from 1000 simulations. Scale indicates substitutions per site. **b**, Models of the canonical mammalian PDK1 and the apicomplexan SPARK proteins. The kinase domains, mammalian pleckstrin homology (PH) domain, and conserved apicomplexan MKXGFL motif are shown. **c**, SPARK-AID was visualized by immunofluorescence microscopy and immunoblotting using the V5 epitope. SPARK-AID was undetectable after 24 h of IAA treatment. Staining for CDPK1 was used to identify parasites, and nuclei were stained with DAPI. Channels adjusted equivalently across all samples. **d**, SPARK-AID depletion, as in **c**, monitored by immunoblot. SPARK-AID is expected to run at 98 kDa.

like kinases, but only one paralog has the N-terminal motif. This suggests the SPARK clade may have arisen from gene duplication prior to the split of the Apicomplexa from other Alveolata, followed by loss of the more closely-related PDK1 homologues in the parasitic clade.

SPARK displayed a diffuse cytosolic localization by immunofluorescence and was depleted without affecting replication after 24 h of IAA treatment in the conditional mutant (**Fig. 7c–7d**; **Extended Data Fig. 5a**; **Supplementary Fig. 3**). Since egress shares several signaling pathways with invasion, I examined the role of SPARK in this process. I induced parasite egress from host cells with the phosphodiesterase inhibitor zaprinast, which increases cGMP levels, activates PKG, and triggers release of intracellular Ca^{2+} stores[45,96–98,183,184]. The Ca^{2+} ionophore A23187 provides an alternative trigger for egress, which also increases cytosolic Ca^{2+} but circumvents guanylate cyclase activity[40,42,43]. Although SPARK knockdown completely blocked zaprinast-induced egress (**Fig. 8a**), it appeared almost entirely dispensable for A23187-induced egress (**Fig. 8b**). These results suggest that SPARK loss interferes with the ability of PKG to trigger intracellular Ca^{2+} release.

To examine SPARK's role in Ca^{2+} release, I tagged the endogenous gene with a HiT vector carrying an mCherry-mAID epitope in parasites expressing TIR1 and the genetically-encoded fluorescent Ca^{2+} sensor GCaMP6f[185]. Treatment of GCaMP6f/SPARK-AID parasites with IAA attenuated cytosolic Ca^{2+} fluxes in intracellular parasites following zaprinast-stimulation (**Fig. 8c–d**). This phenotype was also rescued by A23187. Since cytosolic Ca^{2+} can originate from multiple sources[41,57], I stimulated extracellular parasites in a buffer containing basal Ca^{2+} concentrations (~100 nM free Ca^{2+}). SPARK knockdown blocked zaprinast-induced release of intracellular Ca^{2+} stores (**Fig. 8e**). By contrast, the response to the Ca^{2+} ionophores A23187 or ionomycin was unchanged (**Extended Data Fig. 5b**), indicating that intracellular Ca^{2+} stores are intact but unresponsive to zaprinast in the absence of SPARK. These results establish SPARK as a regulator of the parasite intracellular Ca^{2+} store discharge that precedes both

invasion and egress. I therefore named the kinase “Store Potentiating/Activating Regulatory Kinase” (SPARK), to describe its proposed role in apicomplexan biology.

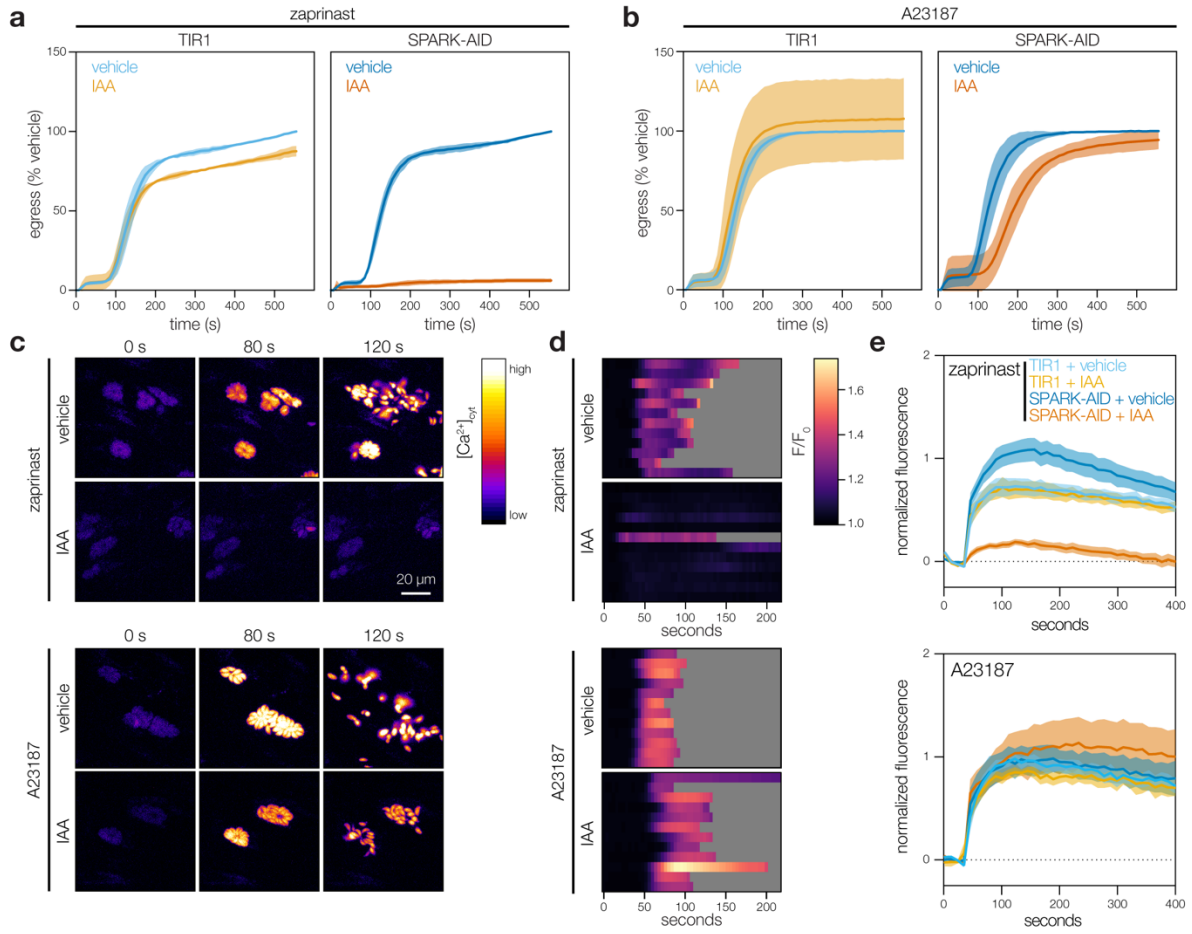

Figure 8. SPARK regulates egress and invasion through modulation of intracellular Ca^{2+} stores. a–b, Parasite egress stimulated with zaprinast (**a**) or the Ca^{2+} ionophore A23187 (**b**) following 24 h of treatment with vehicle or IAA. Egress was monitored by the number of host cell nuclei stained with DAPI over time. Mean graphed for *n* = 3 biological replicates. Shaded regions represent ± S.D. **c**, Selected frames from live video microscopy of zaprinast- or A23187-stimulated SPARK-AID parasites expressing the genetically encoded Ca^{2+} sensor GCaMP6f. Parasites were grown for 24 h with vehicle or IAA prior to the stimulation of egress. **d**, Kymographs showing normalized fluorescence per vacuole relative to the initial intensity, for 12 vacuoles per strain from the experiments in **c**. Gray areas represent the period following egress of the vacuole under observation. **e**, Extracellular parasites in basal Ca^{2+} buffer stimulated with zaprinast or the Ca^{2+} ionophore A23187, following 24 h of treatment with vehicle or IAA. Cytosolic Ca^{2+} flux was measured in bulk as GCaMP6f fluorescence normalized to the initial and maximum fluorescence following aerolysin permeabilization in 2 mM Ca^{2+}. Mean ± S.E. graphed for *n* = 3–6 biological replicates.

Discussion

The temporal resolution of the HiT screens revealed genes displaying a delayed-loss phenotype, including SPARK (TGGT1_268210). The proposed name for the kinase reflects its role in the regulation of Ca^{2+} stores during the parasite lytic cycle. SPARK is critical for egress and release of intracellular Ca^{2+} stores following stimulation of the cGMP pathway—phenotypes rescued by Ca^{2+} ionophores. This pattern mirrors the regulation of filamentous actin translocation during parasite motility (F-actin flux)[186], required for invasion and egress. Regulation of Ca^{2+} stores by proteins such as SPARK likely precedes microneme discharge, and subsequent egress and invasion. However, SPARK's phenotype is distinct from PKG, loss of which cannot be compensated by Ca^{2+} ionophores[46]. This is consistent with models in which PKG regulates the production of diacylglycerol (DAG) and inositol trisphosphate (IP_3)[40,44,47,49,53,187]. IP_3-stimulated release of intracellular Ca^{2+} stores and DAG conversion to phosphatidic acid (PA) are both thought to mediate secretion of microneme contents[188]. Altering the activity of the cGMP-producing guanylate cyclase (GC) blocks zaprinast- and BIPPO-induced egress. Reports differ on the effect of A23187 following GC knockdown—ranging from a nearly normal egress to a complete block[40,42,43]—making it difficult to definitively place SPARK in the pathway.

The observed phenotypes appear inconsistent with the canonical role of PDK1 activating other AGC kinases[87,189]. Failure to activate PKG would block both zaprinast- and ionophore-stimulated egress[96]. Analogously, failure to activate PKA, a negative regulator of egress, would result in premature egress[99,100]. Whether global downregulation of AGC kinase function would phenocopy the loss of SPARK therefore remains an open question. Our study places SPARK as a positive regulator of invasion and egress via potentiation or activation of intracellular Ca^{2+} stores, which could be achieved via direct stimulation of Ca^{2+} channels or modulation of upstream regulators such as PKA. Further work will be needed to distinguish between these models. The characterization of SPARK provides a crucial molecular handle to study the activation of intracellular Ca^{2+} stores—an event that mediates key transitions in the apicomplexan life cycle.

CHAPTER 4: FUTURE DIRECTIONS

The future of HiT screening

HiT screens are a powerful new tool for exploring the apicomplexan genome. While I chose to focus on the *T. gondii* kinome, the technology could be immediately applied to other gene sets of interest. Protein phosphatases, for instance, represent the predominant counteracting force of kinases within the cell and it is the balance between the two that dictates shifts in a cell's signaling network. One such phosphatase, PP1, has already been characterized in *Plasmodium* spp., emphasizing the importance of this protein class on the apicomplexan signaling landscape[190,191]. Alternatively, the previous genome-wide knockout screen identified a class of genes named indispensable conserved apicomplexan proteins (ICAPs)[140]. ICAPs are conserved exclusively within the apicomplexan phylum and are highly fitness-conferring. This class likely represents genes critical to the unique biology and life cycles of the phylum, but consequently many ICAPs lack protein domain and functional annotations. The spatiotemporal resolution of HiT screens makes it a powerful tool for providing potential functional insight into such cryptic gene sets.

The HiT screening platform is amenable to a wide variety of biological questions. By altering the conditional regulation system, gene sets incompatible with the AID system can be assayed. The U1 conditional knockdown system would provide inducible control over genes regardless of their subcellular localization[136]. The HiT vectors could also be redesigned to tag the N terminus of proteins, in order to probe proteins that may be refractory to C-terminal tagging. HiT vectors targeting the 5′ end of genes can further be utilized to replace the promoters of target genes with synthetic promoters of differing strengths. This would enable the study of gene dosage effects in a pooled setting, similar to the CRISPRa screens which have not been successfully adapted to *T. gondii*, to date.

Future iterations of the HiT system may not be limited to localization assignments via arrayed microscopy either. The split-GFP system could enable high-throughput screening of compartmentalization via flow cytometry. By transfecting HiT vectors

containing GFP_{11} into parasites expressing $GFP_{1–10}$ within a desired subcellular compartment, fluorescence signals could be used to sort, sequence, and genotype cells that are colocalizing the two components, and therefore fluorescent. This method could be deployed on a pooled population and would not require the labor-intensive process of arraying.

Recent advances in *in situ* sequencing also raise the possibility of merging the HiT system's throughput of pooled screens with the microscopy-based localization and phenotype characterization of arrayed screens. High-content imaging and *in situ* sequencing has recently been combined to phenotype the effects of a library of gene perturbations in a pooled setting[192]. Adapting this technology to the HiT system would eliminate the need to generate arrays, greatly reducing a critical bottleneck and increasing throughput. The HiT system's spatiotemporal resolution and potential adaptations make it a powerful and promising tool for dissecting the genome of *T. gondii*.

Unanswered questions of SPARK biology

The identification of SPARK provides a novel molecular handle with which to study the invasion and egress pathway of *T. gondii*. I have established SPARK as an upstream regulator of parasite intracellular Ca^{2+} stores. Knockdown of SPARK causes severe defects in the ability of parasites to complete the lytic cycle, indicating that it is a critical component for the proper regulation of the egress and invasion signaling network. Its conservation across the phylum and predicted essentiality in *Plasmodium* spp. indicates a likely conserved function, as is the case with other genes lying in the Ca^{2+} signaling pathway.

How SPARK regulates the release of parasite intracellular Ca^{2+} stores remains unknown. While SPARK possesses a predicted active kinase domain, it is unknown whether kinase activity is responsible for the observed phenotypes. Demonstration of kinase activity *in vitro* with recombinant SPARK protein would provide definitive proof of an active kinase domain. Complementation of the SPARK-AID line with a kinase-dead allele would

determine whether this kinase activity is responsible for SPARK's role in the Ca^{2+} release pathway and other associated phenotypes.

SPARK contains multiple other features of functional interest. The MKXGFL motif is highly conserved amongst SPARK orthologues. The C-terminal tail of SPARK is predicted to be highly structured and predominantly alpha-helical[193]. In contrast to the N-terminal MKXGFL motif, the sequence of the C-terminal tail is not strongly conserved across the phylum. This may indicate divergences in some aspects of SPARK regulation between organisms. Complementation of the SPARK-AID line with truncations or mutations of these domains, in tandem with *in vitro* kinase assays of recombinant mutants, will help to establish the role of these domains on both kinase activity and the involved biological pathways.

A more definitive placing of SPARK's position within the signaling pathway will require systems-level approaches. While SPARK's closest mammalian ortholog is PDK1, it is unclear if SPARK shares a conserved role as a regulator of other AGC kinases. Phosphoproteomics will identify the relevant downstream signaling components. The generation of a SPARK strain with a mutated gatekeeper residue, such as has been achieved for CDPK1, would enable the identification of direct substrates via thiophosphorylation approaches[194]. In tandem, global phosphoproteomics following SPARK knockdown will identify perturbations to both direct and indirect SPARK substrates. Co-immunoprecipitation followed by mass spectrometry experiments will identify interacting partners of SPARK, which may lend insight into modes of regulation or a larger signaling complex in which SPARK partakes. These proteomic approaches will aid in deciphering the SPARK signaling network and provide critical insight into its molecular mechanism of action.

In summation, while SPARK represents a significant addition to our understanding of the requirements for invasion and egress, many questions remain in regards to the overall topology of the signaling network. The identification of SPARK now provides a previously unknown molecular handle with which to answer these questions. Understanding

SPARK's role within the Ca^{2+} signaling pathway is critical for deciphering the molecular events that govern apicomplexan pathogenesis.

Concluding remarks

In this thesis I have described the development of a novel high-throughput screening platform in *T. gondii*. In **Chapter 2** I describe the validation of this system and its use to profile the parasite kinome. By utilizing both a fluorophore and a conditional degron system I was able to localize proteins to subcellular compartments and phenotype the effect of protein knockdown via high-throughput arrayed screening. Pooled screens enabled increased temporal resolution that was not observed in previous knockout screens. In **Chapter 3** I characterized SPARK, a gene identified by the HiT screens as a delayed-loss candidate. SPARK is essential for completing the parasite lytic cycle and serves as a positive regulator of parasite intracellular Ca^{2+} release. The identification and characterization of SPARK is an important addition to our knowledge of this signaling network.

Apicomplexan parasites remain some of the most widespread and medically significant pathogens on the planet. The development of novel tools and approaches for studying these highly diverged organisms will be critical to our success in understanding their biology and developing novel therapeutics against them. The work in this thesis represents a step towards this ultimate goal.

METHODS

Data analysis

All data analysis was performed in either Microsoft Excel (version 16.58), GraphPad Prism (version 9.1.2), RStudio (version 1.2.5033), Perl (version 5.18), FlowJo (version 10.7), ImageJ (version 2.0.0), or SnapGene (version 5.1.5).

Parasite and host cell culture

T. gondii parasites were grown in human foreskin fibroblasts (HFFs) maintained in DMEM (GIBCO) supplemented with 3% inactivated fetal calf serum (IFS) and 10 µg/mL gentamicin (Thermo Fisher Scientific), referred to as D3. Where noted, DMEM supplemented with 10% IFS and 10 µg/mL gentamicin was used, referred to as D10.

Parasite transfection

Parasites were passed through 3 µm filters, pelleted at 1000 × *g* for 10 min, washed, resuspended in Cytomix (10 mM KPO_4, 120 mM KCl, 150 mM $CaCl_2$, 5 mM $MgCl_2$, 25 mM HEPES, 2 mM EDTA, 2 mM ATP, and 5 mM glutathione), and combined with transfected DNA to a final volume of 400 µL. Electroporation used an ECM 830 Square Wave electroporator (BTX) in 4 mm cuvettes with the following settings: 1.7 kV, 2 pulses, 176 µs pulse length, and 100 ms interval.

Strain generation

Oligos were ordered from IDT. All cloning was performed with Q5 2X master mix (NEB) and NEBuilder HiFi assembly (NEB) unless otherwise noted. Primers and plasmids used or generated in this study can be found in (**Supplementary Table 1**). Oligos, plasmids, and strains generated within this study are available from the corresponding author by request.

Scarless CDPK1-mNG-AID. The V5-TEV-mNeonGreen-AID-Ty cassette was PCR amplified from plasmid pBM050 with repair homology arms using primers P108 and P109. Oligos P110 and P111 were duplexed and cloned into plasmid pSS013 to create

the gRNA/Cas9-expression plasmid. The gRNA/Cas9-expression plasmid was co-transfected with the repair template into TIR1 parasites[46,61]. Following the first lysis, mNeonGreen positive clones were isolated via fluorescence-activated cell sorting. Single clones were obtained by limiting dilution and verified by PCR amplification using primers P114 and P115 and sequencing with primers P112 and P113.

Scarless CDPK3-mNG-AID. The CDPK3-mNG-AID scarless strain was generated as CDPK1-mNG-AID above, using primers P116 and P117 for repair template amplification, oligos P118 and P119 for assembly of the gRNA/Cas9-expression plasmid, primers P120 and P121 for validation of clonal isolates, and primers P112 and P113 for the sequencing of tag junctions.

TIR1/IMC1-tdTomato. The sequence pTUB1_IMC1-tdTomato_DHFR was PCR-amplified with primers P96 and P97 to yield a repair template with homology to a defined, neutral genomic locus[195]. Approximately 2 x 10^7 extracellular TIR1 parasites were transfected with 50 µg gRNA/Cas9 plasmid targeting the neutral locus and 6 µg of repair template. Single clones were isolated by fluorescence-activated cell sorting into 96-well plates containing HFFs. IMC1-tdTomato positive clones were subsequently identified by microscopy and verified by PCR amplification of the locus using primers P98 and P99.

TGGT1_268210, TGGT1_204280, TGGT1_239885, and TGGT1_239420 AID-tagged lines. HiT vector cutting unit gBlocks (IDTDNA) (P122–125) were cloned into the pGL015 mNeonGreen HiT vector backbone. HiT vectors were linearized with BsaI and co-transfected with the pSS014 Cas9-expression plasmid into TIR1 parasites. Clones were selected with pyrimethamine and isolated via limiting dilution. Clones were verified by PCR amplification and sequencing of the junction between the 3′ end of the gene (P100-P103) and 5′ end of the protein tag (P104 for TGGT1_268210 and P105 for TGGT1_204280, TGGT1_239420, and TGGT1_239885).

TIR1/GCaMP6f. The primers P106 and P107 were used to PCR-amplify the sequence pTUB1-GCaMP6f-DHFR3′UTR from plasmid Genbank MT345687 to yield a repair template with homology to the 5′ and 3′ ends of a defined, neutral genomic locus[195].

Approximately 1×10^7 extracellular parasites were transfected with 25 µg gRNA/Cas9-expression plasmid pBM041 and 5 µg GCaMP6f repair template. Following two rounds of fluorescence-activated cell sorting, GFP-positive clones were isolated by limiting dilution.

TIR1/GCaMP6f/268210-AID. The TGGT1_268210 HiT vector cutting unit gBlock (IDTDNA) was cloned into the pALH052 V5-TEV-mCherry-AID HiT vector backbone. The HiT vector was linearized with BsaI and co-transfected with the pSS014 Cas9-expression plasmid into TIR1/GCaMP6f parasites. Parasite populations were selected with 25 µg/mL mycophenolic acid and 50 µg/mL xanthine. Single clones were isolated by limiting dilution. Clones were verified by sequencing of the junction between the 3′ end of the gene and 5′ end of the protein tag.

Analysis of CDPK1- and CDPK3-tagged HiT vector populations

Parasites were co-transfected with 40–50 µg of BsaI-linearized HiT $3'_{SAG1}$ or HiT $3'_{CDPK3}$ vectors and the Cas9-expression plasmid pSS014. 24 h post-transfection parasite populations were selected with 3 µM pyrimethamine. Following selection populations were analyzed by flow cytometry with a Miltenyi MACSQuant VYB. Populations were imaged by microscopy using a 60X objective and an Eclipse Ti microscope (Nikon) with an enclosure maintained at 37°C and 5% CO_2. For IAA-induced depletion experiments, intracellular parasites were treated with either 50 µM IAA or an equivalent dilution of PBS for 24 h. Following treatment, parasites were passed through a 27-gauge needle, isolated by filtration, and analyzed by flow cytometry.

Design and cloning of HiT vector libraries

Three gRNA constructs were designed against each gene in the 155 gene library. Since the efficiency of recombination decreases with the distance of the homology regions from the double-stranded break, I selected gRNAs that cut within a 50 bp window downstream of the stop codon[196–199]. The 3′ end of the genomic sequences (release 36, ToxoDB.org) were scanned for gRNAs containing either NGG or NAG PAMs. gRNAs were ranked based on predicted on-target activity and off-target activity, as determined

by the Rule Set 2 and Cutting Frequency Determination calculators[169], respectively, and by the distance of the cutsite from the stop codon. As the Rule Set 2 calculator does not take into account efficiencies of different PAMs, the on-target scores of NAG gRNAs were penalized as predicted by the Cutting Frequency Determination calculator. These ranks were used to create an aggregate rank for gRNA selection. Initially, only the highest-ranking gRNAs were selected with cut sites within 30 bp of the stop codon and with a Rule Set 2 score above 0.2. The criteria were progressively relaxed to allow any gRNA within 30 bp, any gRNA within 50 bp and with a Rule Set 2 score above 0.2, and finally any gRNA within 50 bp, until each gene had 3 gRNAs assigned. A 'G' was preprended to gRNAs that did not start with one to ensure proper RNA polymerase III initiation. Synonymous point mutations were introduced to H1 homology regions containing BsaI or AscI restriction sites, in order to prevent restriction enzyme cutting during the cloning process. The guide library was synthesized by Agilent and each oligo includes a gRNA, 40 bp homology regions, an AscI restriction site for insertion of the gRNA scaffold, and tandem BsaI sites for linearization of the final constructs, all flanked by sequences for cloning into empty HiT vectors (**Supplementary Table 1**). The HiT 3′$_{SAG1}$ and HiT 3′$_{CDPK3}$ libraries were cloned as described below. The HiT 3′$_{CDPK3}$ library protocol resulted in both a slight increase of correctly assembled products and greater library diversity. All PCR steps were performed with iProof High-Fidelity DNA polymerase (Bio-Rad) and cloning products were electroporated into MegaXDH10B T1R electrocompetent cells.

HiT 3′$_{SAG1}$ library. The synthesized oligo library was PCR amplified with primers P1 and P2. PCR products were cloned into the pTS018 entry vector via Gibson assembly (VWR). The gRNA scaffold was amplified from pSL001 with primers P3 and P4. The amplified scaffold was inserted into AscI-digested entry vector library via NEBuilder HiFi assembly. Finally, the assembled cutting units were PCR amplified using primers P1 and P2 and cloned into pTS020, the mNeonGreen-AID HiT 3′$_{SAG1}$ vector, via NEBuilder HiFi assembly. DNA products were isolated from liquid cultures using either a ZymoPURE II Plasmid Maxiprep Kit (Zymo Research) or a Macherey-Nagel Nucleobond Xtra Maxi Kit.

HiT 3′$_{CDPK3}$ library. In order to decrease polymerase-induced errors I replaced PCR amplification steps with digestion with the type IIS restriction enzyme BsrDI. The oligo library was PCR amplified with primers P1 and P2, as in the HiT 3′$_{SAG1}$ library. PCR products were cloned into the pTS031 entry vector via NEBuilder HiFi assembly. The gRNA scaffold was isolated from pTS028 via BsrDI digestion and inserted into AscI-digested entry vector library. Finally, the assembled "cutting units" were BsrDI-digested out of the entry vector library and cloned into pGL015, the mNeonGreen-AID HiT 3′$_{CDPK3}$ vector. DNA products were isolated from solid agar plate cultures using a ZymoPURE II Plasmid Maxiprep Kit.

Pooled HiT vector screening

For each screen, 500 µg of the HiT vector library was linearized with BsaI-HFv2, cleaned-up using Agencourt RNAClean XP SPRI paramagnetic beads, and co-transfected with the Cas9-expression plasmid pSS014 into 5 x 10^8 TIR1 parasites in the HiT 3′$_{SAG1}$ screen and 5 x 10^8 TIR1/IMC1-tdTomato parasites in the HiT 3′$_{CDPK3}$ screen. Transfected parasites were used to infect 12 and 10 15-cm^2 dishes with HFF monolayers in the HiT 3′$_{SAG1}$ and 3′$_{CDPK3}$ screens, respectively. 3 µM pyrimethamine and 10 µg/mL DNaseI was added 24 h later. The parasites were allowed to egress naturally from host cells, isolated by filtration, and passaged onto 8 15-cm^2 dishes with fresh monolayers. This process was repeated for two more passages, infecting each dish with approximately 2–3 x 10^7 parasites. Following the third passage, the population was split into three 15 cm^2 dishes containing fresh monolayers in D10 supplemented with 50 µM IAA and 3 15-cm^2 dishes supplemented with an equal dilution of vehicle (PBS). The populations were maintained and passaged in their respective conditions for three passages in the HiT 3′$_{SAG1}$ screen and for four passages in the HiT 3′$_{CDPK3}$ screen. At select passages approximately 10^8 parasites were pelleted and stored at -80°C for analysis. Parasite DNA was extracted using the DNeasy Blood and Tissue kit (QIAGEN) and integrated gRNA constructs were amplified with primer P5 and barcoding primers P6–22. The resulting libraries were sequenced using a MiSeq v2 kit (Illumina) with single-reads using custom sequencing primer P23 and custom indexing primer P24.

Sequencing reads were aligned to the gRNA library. Read counts were median normalized and gRNAs in the bottom 5th percentile of the input library were removed. To account for differences in NGG and NAG PAM efficiencies, relative abundances for each gRNA were corrected for the PAM used. The PAM efficiencies were calculated by comparing the abundances of only gRNAs in the selected population that target genes identified as dispensable in a previous genome-wide knockout screen[140]. Fold-changes were normalized to passage 2. UMAP was used to compare gRNAs in each screen based on their pattern of fold changes for vehicle- and IAA-treated samples. Clusters were calculated by k-means. Gene centroids were calculated in UMAP space and assigned to the dispensable or fitness-conferring class using k-means clustering.

Arrayed HiT vector screening

Generation and passaging of array. In parallel to the pooled HiT $3'_{CDPK3}$ screen, single clones were isolated via limiting dilution after 4 passages of drug selection. Parasites from passage 4 were collected and sequenced as in the pooled screening experiments, using primer P5 and P25 for PCR amplification. 1160 clonal isolates were arrayed into twenty 96-well plates containing HFFs. Included in each plate was a well containing the TIR1/IMC1-tdTomato parental line and a well containing the CDPK1-AID scarless strain. Arrays were passaged every 3 days with a multichannel pipette by transferring 5% of the total lysed well volume to 96-well plates containing HFF monolayers. Individual wells with incomplete lysis were scraped and passed with 10% of the total well volume.

Arrayed widefield microscopy. Freshly lysed arrays were replica plated with 12 µL into 96-well plates of HFFs maintained in FluoroBrite DMEM (GIBCO) supplemented with 3% IFS, 4 mM glutamine, and 10 mg/mL gentamicin. Replica plates were centrifuged at 150 × *g* and 18°C for 5 min and subsequently incubated at 37°C and 5% CO_2. At 3 h post-infection, replica plates were supplemented with either PBS or IAA to a final concentration of 50 µM. At 24 h post-IAA or PBS addition, each well was imaged at 4 adjacent fields-of-view using a 40X objective and an Eclipse Ti microscope (Nikon) with an enclosure maintained at 37°C and 5% CO_2. Images were acquired using the NIS

elements imaging software, W-View Gemini image splitting optics, and a Zyla 4.2 sCMOS camera. FIJI software was used for image analysis and processing.

Arrayed lytic assays. Freshly lysed arrays were replica plated with 10 µL into 96-well plates of HFFs maintained in D3 supplemented with either 50 µM IAA or PBS. Each replica plate contained 6 uninfected control wells. Replica plates were centrifuged at 150 × *g* and 18°C for 5 min and incubated for 72 h at 37°C and 5% CO_2. Plates were washed 1X with PBS and fixed for 10 minutes with 100% ethanol. Intact monolayers were visualized by staining the plates for 5 min with crystal violet solution (12.5 g crystal violet, 125 mL 100% ethanol, 500 mL 1% ammonium oxalate) followed by two PBS washes, one water wash, and overnight drying. Absorbance at 590 nm was read as a measure of host cell lysis and normalized to the average of a plate's uninfected control wells.

Dual-indexed sequencing of arrays. Parasites were harvested from 100 µL of lysed wells by centrifugation at 1000 × *g* and 18°C for 10 min. Pellets were each resuspended in 25 µL of lysis buffer (1X Q5 buffer supplemented with 0.2 mg/mL Proteinase K) and lysed using the following conditions: 37°C for 1 h, 50°C for 2 h, and 95°C for 15 min. Guides were PCR-amplified from gDNA, with each well utilizing a unique combination of i7 index primers (P26–65) and i5 index primers (P66–95). PCR products from an individual plate were pooled and gel extracted using a Zymoclean Gel DNA Recovery Kit and subsequently pooled at equimolar ratios for sequencing. The final PCR product pool was sequenced with a MiSeq v2 kit (Illumina) using dual-indexed single-reads with primers P23 and P24. Sequencing reads were aligned to the gRNA library. A well was designated as gRNA-containing if a single gRNA had more than 100 reads. Wells containing multiple integrations or mixed populations were defined as those in which a secondary gRNA contained more than 10% the number of reads assigned to the most abundant gRNA.

Confocal microscopy of select clones

Parasites were inoculated into 96-well glass-bottom plates (Cellvis) of HFFs maintained in FluoroBrite DMEM supplemented with 10% IFS, 4 mM glutamine, and 10 µg/mL gentamicin. At 24 h post-infection wells were imaged with an RPI spinning disk confocal

microscope and a 63x objective maintained at 37°C and 5% CO_2. Images were acquired using the MetaMorph acquisition software and a Hammamatsu ORCA-ER CCD camera. The parental TIR1/IMC1-tdTomato strain was also imaged to control for background fluorescence. ImageJ was used for image analysis and processing.

Plaque assays

Parasites were inoculated into 6-well plates of HFFs maintained in D10 and allowed to grow undisturbed for 9 days. For AID strains the cells were maintained in either 50 μM IAA or PBS. For the CDPK1-HA-U1 population the cells were treated with a 2-hour pulse of either 50 nM rapamycin or DMSO at 24 hours post-infection. The rapamycin and DMSO were subsequently washed out and the cells were grown in D10 for the remainder of the assay. Plates were washed with PBS and fixed for 10 min at room temperature with 100% ethanol. Plates were stained with crystal violet solution for 5 min at room temperature, followed by two washes with PBS, one wash with water, and drying. Plaque area calculations were performed in ImageJ.

Competition assays

Freshly lysed strains were filtered through 5 μm filters and pelleted at 1000 x *g* and 18°C for 10 min. Pellets were resuspended in D10 and counted. T12.5s of HFFs were infected with 1.5 x 10^6 parasites of the TIR1/IMC1-tdTomato strain and 1.5 x 10^6 parasites of the competitor strain. At 24 h post-infection the media was changed with fresh D10. Populations were assayed by flow cytometry following host cell lysis, and each population was passed to two wells of a 6-well plate. At 24 h post-infection the media of one well per strain was changed to D10 and vehicle (PBS) and the media of the second well changed to D10 and 50 μM IAA. Populations were maintained in these conditions for four passages. Following each lysis, the populations were assayed by flow cytometry with a Miltenyi MACSQuant VYB. The fraction of the population that was tdTomato negative was represented as a ratio of the [% tdTomato negative in the IAA sample]/[% tdTomato negative in the vehicle sample] and was normalized to the initial fraction pre-splitting into ± IAA media.

Invasion assays

Strains were each passed to two flasks of HFFs containing D10 media. At 3 h post-infection one flask was supplemented with vehicle (PBS) and the second flask was supplemented with IAA to a final concentration of 50 µM. At 27 h post-infection each flask was syringe-lysed and filtered through 5 µm filters. Parasites were pelleted at 1000 x *g* and 18°C for 10 min. Pellets were resuspended in invasion media (HEPES-buffered DMEM without phenol red) supplemented with 1% IFS to a concentration of 1 x 10^6 parasites/mL. 200 µL of each parasite solution was added to 3 wells of a clear-bottom 96-well plate containing HFFs. The plate was centrifuged at 290 x *g* and room temperature for 5 min. Plates were incubated for 10 min at 37°C to stimulate invasion. Following incubation wells were fixed with 4% formaldehyde and extracellular parasites were stained with mouse anti-SAG1 antibody diluted 1:500[200]. All parasites were stained by permeabilizing with 0.25% Triton X-100 and staining with guinea pig anti-CDPK1 diluted 1:10,000 (Covance[70]). Cells were subsequently stained with anti-guinea pig Alexa-594 antibody diluted 1:1000 (Invitrogen), anti-mouse Alexa-488 antibody diluted 1:1000 (Invitrogen), and Hoechst 33258 (Santa Cruz Biotechnology) nuclear dye. Samples were imaged using a Biotek Cytation3 imaging multimode reader. The number of invaded parasites per field of view was counted and normalized to the number of host cells in the same area. The invasion efficiency for each replicate was normalized to the invaded parasites per host cell nuclei of the parental TIR1 vehicle sample.

Phylogenetic analysis of SPARK

SPARK homologs were identified by BLAST search against representative apicomplexan genomes. Protein kinase domains were obtained from EupathDB based on their annotation with Interpro domain IPR011009. Sequences were curated for *Theileria* spp., *Cryptosporidium parvum*, *Cryptosporidium hominis*, *Sarcocystis neurona*, *Vitrella brassicaformis*, and *Chromera velia* to correct errors in the gene model. Domains from the nearest human, mouse, and macaque orthologues (as determined by BLAST) were used as outgroups. Individual domains were aligned using ClustalX2, and the

phylogenetic tree was generated by neighbor-joining. Visualizations were generated using FigTree (v1.4.4).

Immunoblotting

For detecting SPARK depletion, TIR1 and SPARK-AID parasites were grown in D10 for 3 h before being treated with either 50 µM IAA or vehicle (PBS). After 24 h of treatment, parasites were passed through 27-gauge needles and isolated via filtration. Parasites were resuspended in lysis buffer (0.8% IGEPAL-CA630, 0.25 U/µL benzonase, and 2X Halt Protease Inhibitor Cocktail in PBS) and incubated on ice for 15 min. Lysates were combined with 1X Laemmli buffer (diluted from 5X buffer containing 10% SDS, 50% glycerol, 300 mM Tris HCl pH 6.8, 0.05% bromophenol blue) with 1% final volume β-mercaptoethanol and boiled for 10 min. Samples were run on a 7.5% SDS-PAGE gel (BioRad) and transferred onto a nitrocellulose membrane in transfer buffer (25 mM Tris-HCl, 192 mM glycine, 20% methanol). Blocking and all subsequent antibody incubations were performed at room temperature in 5% milk in TBS-T (20 mM Tris, 138 mM NaCl, 1 L PBS, 0.1% Tween-20) unless otherwise noted. The blot was incubated in blocking buffer for 1 h followed by incubation with the mouse anti-V5 primary antibody diluted 1:2000 (R960-25, Invitrogen) for 1 h. The blot was washed three times with TBS-T and incubated for 1 h with the anti-mouse secondary antibody diluted 1:10,000 (LI-COR). Following imaging the blot was incubated overnight at 4°C with the guinea pig anti-CDPK1 primary antibody diluted 1:100,000 (Covance)[70]. The blot was washed three times with TBS-T, incubated for 1 h with anti-guinea pig secondary antibody diluted 1:10,000 (LI-COR), washed 3X with TBS-T, and imaged using a LI-COR Odyssey CLx.

For detecting CDPK1-V5-T2A-mKate2, Δ*ku80* and the transfected population were harvested from fully lysed host cells. Parasites were lysed, run on a 4–15% gradient SDS-PAGE gel (BioRad), and transferred onto a nitrocellulose membrane as above. The blot was incubated for 1 h with mouse anti-V5 primary antibody diluted 1:2000 (R960-25, Invitrogen) and rabbit anti-RFP primary antibody diluted 1:4000 (R10367, Life Technologies). The blot was washed three times with TBS-T and incubated for 1 h with anti-mouse and anti-rabbit secondary antibodies diluted 1:10,000 (LI-COR). Following

imaging the blot was incubated with rabbit anti-ALD1 primary antibody diluted 1:10,000 (Zymed Laboratories Inc.)[201], for 1 h. Following three washes with TBS-T, the blot was incubated for 1 h with anti-rabbit secondary antibodies diluted 1:10,000 (LI-COR), washed 3X with TBS-T, and imaged.

Immunofluorescence assays

Parasites were inoculated onto coverslips containing HFFs. For AID strains, after 3 h cells were treated with either 50 µM IAA or PBS. At 24 h post-treatment, intracellular parasites were fixed with 4% formaldehyde and permeabilized with 0.25% Triton X-100 in PBS. For the CDPK1-HA-U1 population, after 3 h cells were treated with either 50 nM rapamycin or DMSO for 2h. At 24 h post-rapamycin pulse, intracellular parasites were fixed and permeabilized as above. Nuclei were stained with Hoechst 33342 or Hoescht 33258 (Santa Cruz) and coverslips were mounted in Prolong Diamond (Thermo Fisher). V5 was detected using a mouse monoclonal antibody (R960-25, Invitrogen). CDPK1 was detected using a guinea pig-derived polyclonal antibody diluted 1:10,000 (Covance)[70]. HA was detected using a mouse monoclonal antibody diluted 1:1000 (901501, BioLegend). GAP45 was detected using a rabbit polyclonal antibody diluted 1:1000 (Eurogentec)[202]. Primary antibodies were stained with anti-guinea pig, anti-mouse, or anti-rabbit Alexa-Fluor-labeled secondary antibodies diluted 1:1000 (Invitrogen). Images were acquired with an Eclipse Ti microscope (Nikon) using the NIS elements imaging software and a Zyla 4.2 sCMOS camera. ImageJ was used for image analysis and processing.

Replication assays

Parasites were inoculated onto coverslips containing HFFs and after 3 h were treated with either 50 µM IAA or PBS. At 24 h post-IAA addition, intracellular parasites were fixed, permeabilized, and stained and imaged as described under *Immunofluorescence assays*. For each sample, multiple fields of view were acquired. The number of parasites per vacuole were calculated from 100 vacuoles. Results are the mean of three independent experiments.

Egress assays

Egress was quantified in a plate-based manner[203]. HFF monolayers in a clear-bottomed 96-well plate infected with 7.5 $\times 10^4$ parasites per well of parental or SPARK-AID for 3 h were treated with 50 µM IAA or PBS for an additional 24 h. Before imaging, the media was exchanged for FluoroBrite supplemented with 10% IFS. Three images were taken before zaprinast (final concentration 500 µM) or A23187 (final concentration 8 µM) and DAPI (final concentration 5 ng/mL) were added, and imaging of DAPI-stained host cell nuclei continued for 9 additional minutes before 1% Triton X-100 was added to all wells to determine the total number of host cell nuclei. Imaging was performed at 37°C and 5% CO_2 using a Biotek Cytation 3 imaging multimode reader. Results are the mean of three wells per condition and are representative of three independent experiments.

Live cell microscopy of GCaMP6f-expressing parasites

To capture egress, SPARK-AID parasites were grown in HFFs in glass-bottom 35mm dishes (Ibidi) for 3 h at which point they were treated with either 50 µM IAA or PBS for an additional 24 h. Parasites were stimulated to egress with 500 µM zaprinast or 8 µM A23187 in Ringer's buffer prepared without Ca^{2+} (155 mM NaCl, 3 mM KCl, 1 mM $MgCl_2$, 3 mM NaH_2PO_4, 10 mM HEPES, 10 mM glucose) and supplemented with 1% BSA (w/v) and recorded every 4 s for 220 s with an Eclipse Ti microscope (Nikon) in an enclosure maintained at 37°C and 5% CO_2. Images were acquired using the NIS elements imaging software and a Zyla 4.2 sCMOS camera. Image analysis and quantification was done using ImageJ.

Extracellular zaprinast and Ca^{2+} ionophore treatment of GCaMP6f strains

Parasites were passed to 15-cm^2 dishes containing HFFs and after 6 h treated with either 50 µM IAA or vehicle (PBS). Following 24 h of treatment the cells were washed once with PBS and harvested in cold Ringer's Basal Ca^{2+} (155 mM NaCl, 3 mM KCl, 1 mM $MgCl_2$, 3 mM NaH_2PO_4, 10 mM HEPES, 10 mM glucose, 250 µM EGTA, 112 µM $CaCl_2$). Parasites were isolated via syringe lysis and filtration, pelleted and washed once with cold Ringer's Basal Ca^{2+}, and resuspended to 1 x 10^7 parasites/mL. 100 µL of parasite suspension was

added to a clear-bottom 96-well plate and incubated on ice for 5 min. Fluorescence was read with an excitation wavelength of 485 nm and an emission wavelength of 528 nm every 10 s in a BioTek Cytation 3. At 30 s 50 µL of 3X zaprinast (100 µM final concentration), A23187 (2 µM final concentration), ionomycin (1 µM final concentration), or vehicle (DMSO) was added and fluorescence readings were taken for an additional 6 min. 50 µL of 4X aerolysin (3 µg/mL final concentration) and $CaCl_2$ (2 mM final concentration) was added, and the assay plate was incubated at 37°C for 10 min. Fluorescence was read every 1 min for 40 min. The assay plate was shaken for 1 s before each read. The non-fluorescent TIR1 strain was used to perform a baseline subtraction of background fluorescence. Baseline-subtracted values were normalized to initial fluorescence pre-stimulation and maximum fluorescence post-aerolysin treatment. Results are the mean of three independent experiments in the case of A23187 and ionomycin and six independent experiments in the case of zaprinast and DMSO.

DATA AVAILABILITY

Supplementary Table 1, **Supplementary Table 2**, and minimally processed data are available from the reference Smith et al., 2021[204]. All oligos used in this study are available in **Supplementary Table 1**. All plasmids used or generated in this study are listed in **Supplementary Table 1**. Minimally processed pooled and arrayed CRISPR screen sequencing results are available in **Supplementary Table 2**. Localization assignments, microscopy phenotypes, lytic assay results, and UMAP coordinates and clusters are likewise available in **Supplementary Table 2**. Additional unprocessed data is available from the corresponding author upon request.

CODE AVAILABILITY

All code is described in the methods section and available from the corresponding author upon request.

ACKNOWLEDGEMENTS

We thank the Whitehead Institute Bioinformatics and Research Computing Core, especially Bingbing Yuan, for assistance implementing gRNA design pipelines; L. David Sibley for the TIR1 strain; Moritz Treeck for the DiCre strain; Wendy Salmon and the W.M. Keck Biological Imaging Facility for confocal microscopy support; Peter W. Reddien for use of the Illumina MiSeq; Benjamin S. Waldman, Elizabeth A. Boydston, Christopher J. Giuliano, Alex W. Chan, Saima Sidik, and Benedikt M. Markus for technical support in generation of the array; VEuPathDB and all contributors to this resource. This work was supported by funds from a National Institutes of Health grant (R01AI144369) to S.L. and National Science Foundation Graduate Research Fellowships to T.A.S. (2018259980) and A.L.H. (174530).

AUTHOR CONTRIBUTIONS STATEMENT

T.A.S. and S.L. designed the overall study and experiments. HiT vectors were designed, constructed, and tested for their tagging efficiency by T.A.S. and G.S.L. The TIR1/GCaMP6f parasite strain was constructed and validated by A.L.H. and the scarlessly tagged CDPK1 and CDPK3 parasite strains were constructed and validated by E.S. T.A.S. performed all remaining parasite strain construction and experiments. T.A.S. and S.L. wrote the manuscript and all authors reviewed, offered input, and approved the manuscript.

REFERENCES

1. Escalante, A. A. & Ayala, F. J. Evolutionary origin of Plasmodium and other Apicomplexa based on rRNA genes. *Proc. Natl. Acad. Sci. U. S. A.* **92**, 5793–5797 (1995).
2. Levine, N. D. Progress in taxonomy of the Apicomplexan protozoa. *J. Protozool.* **35**, 518–520 (1988).
3. Pawlowski, J. *et al.* CBOL protist working group: barcoding eukaryotic richness beyond the animal, plant, and fungal kingdoms. *PLoS Biol.* **10**, e1001419 (2012).
4. Aly, A. S. I., Vaughan, A. M. & Kappe, S. H. I. Malaria parasite development in the mosquito and infection of the mammalian host. *Annu. Rev. Microbiol.* **63**, 195–221 (2009).
5. Tandel, J. *et al.* Life cycle progression and sexual development of the apicomplexan parasite Cryptosporidium parvum. *Nat Microbiol* **4**, 2226–2236 (2019).
6. Black, M. W. & Boothroyd, J. C. Lytic cycle of Toxoplasma gondii. *Microbiol. Mol. Biol. Rev.* **64**, 607–623 (2000).
7. Koreny, L. *et al.* Molecular characterization of the conoid complex in Toxoplasma reveals its conservation in all apicomplexans, including Plasmodium species. *PLoS Biol.* **19**, e3001081 (2021).
8. Katris, N. J. *et al.* The apical complex provides a regulated gateway for secretion of invasion factors in Toxoplasma. *PLoS Pathog.* **10**, e1004074 (2014).
9. O'Shaughnessy, W. J., Hu, X., Beraki, T., McDougal, M. & Reese, M. L. Loss of a conserved MAPK causes catastrophic failure in assembly of a specialized cilium-like structure in Toxoplasma gondii. *MBoC* **31**, 881–888 (2020).
10. Back, P. S. *et al.* Ancient MAPK ERK7 is regulated by an unusual inhibitory scaffold required for Toxoplasma apical complex biogenesis. *Proc. Natl. Acad. Sci. U. S. A.* **117**, 12164–12173 (2020).
11. Chen, X.-M., Keithly, J. S., Paya, C. V. & LaRusso, N. F. Cryptosporidiosis. *N. Engl. J. Med.* **346**, 1723–1731 (2002).

12. Phillips, M. A. *et al.* Malaria. *Nat Rev Dis Primers* **3**, 17050 (2017).
13. Tenter, A. M., Heckeroth, A. R. & Weiss, L. M. Toxoplasma gondii: from animals to humans. *Int. J. Parasitol.* **30**, 1217–1258 (2000).
14. Weiss, L. M. & Dubey, J. P. Toxoplasmosis: A history of clinical observations. *Int. J. Parasitol.* **39**, 895–901 (2009).
15. Dubey, J. P., Miller, N. L. & Frenkel, J. K. The Toxoplasma gondii oocyst from cat feces. *J. Exp. Med.* **132**, 636–662 (1970).
16. Radke, J. R. & White, M. W. A cell cycle model for the tachyzoite of Toxoplasma gondii using the Herpes simplex virus thymidine kinase. *Mol. Biochem. Parasitol.* **94**, 237–247 (1998).
17. Paredes-Santos, T. C., de Souza, W. & Attias, M. Dynamics and 3D organization of secretory organelles of Toxoplasma gondii. *J. Struct. Biol.* **177**, 420–430 (2012).
18. Kafsack, B. F. C. *et al.* Rapid membrane disruption by a perforin-like protein facilitates parasite exit from host cells. *Science* **323**, 530–533 (2009).
19. Carruthers, V. B. & Sibley, L. D. Mobilization of intracellular calcium stimulates microneme discharge in Toxoplasma gondii. *Mol. Microbiol.* **31**, 421–428 (1999).
20. Wetzel, D. M., Chen, L. A., Ruiz, F. A., Moreno, S. N. J. & Sibley, L. D. Calcium-mediated protein secretion potentiates motility in Toxoplasma gondii. *J. Cell Sci.* **117**, 5739–5748 (2004).
21. Donahue, C. G., Carruthers, V. B., Gilk, S. D. & Ward, G. E. The Toxoplasma homolog of Plasmodium apical membrane antigen-1 (AMA-1) is a microneme protein secreted in response to elevated intracellular calcium levels. *Mol. Biochem. Parasitol.* **111**, 15–30 (2000).
22. Petri W. A. *et al.* Toxoplasma gondii Homologue ofPlasmodium Apical Membrane Antigen 1 Is Involved in Invasion of Host Cells. *Infect. Immun.* **68**, 7078–7086 (2000).
23. Bargieri, D. Y. *et al.* Apical membrane antigen 1 mediates apicomplexan parasite attachment but is dispensable for host cell invasion. *Nat. Commun.* **4**, 2552 (2013).
24. Mordue, D. G., Desai, N., Dustin, M. & Sibley, L. D. Invasion by Toxoplasma gondii establishes a moving junction that selectively excludes host cell plasma

membrane proteins on the basis of their membrane anchoring. *J. Exp. Med.* **190**, 1783–1792 (1999).

25. Mordue, D. G. & Sibley, L. D. Intracellular fate of vacuoles containing Toxoplasma gondii is determined at the time of formation and depends on the mechanism of entry. *J. Immunol.* **159**, 4452–4459 (1997).
26. Katris, N. J., Ke, H., McFadden, G. I., van Dooren, G. G. & Waller, R. F. Calcium negatively regulates secretion from dense granules in Toxoplasma gondii. *Cell. Microbiol.* **21**, e13011 (2019).
27. Franco, M. *et al.* A Novel Secreted Protein, MYR1, Is Central to Toxoplasma's Manipulation of Host Cells. *MBio* **7**, e02231–15 (2016).
28. Schwab, J. C., Beckers, C. J. & Joiner, K. A. The parasitophorous vacuole membrane surrounding intracellular Toxoplasma gondii functions as a molecular sieve. *Proc. Natl. Acad. Sci. U. S. A.* **91**, 509–513 (1994).
29. Gold, D. A. *et al.* The Toxoplasma Dense Granule Proteins GRA17 and GRA23 Mediate the Movement of Small Molecules between the Host and the Parasitophorous Vacuole. *Cell Host Microbe* **17**, 642–652 (2015).
30. Mercier, C. *et al.* Biogenesis of nanotubular network in Toxoplasma parasitophorous vacuole induced by parasite proteins. *Mol. Biol. Cell* **13**, 2397–2409 (2002).
31. Sibley, L. D., Niesman, I. R., Parmley, S. F. & Cesbron-Delauw, M. F. Regulated secretion of multi-lamellar vesicles leads to formation of a tubulo-vesicular network in host-cell vacuoles occupied by Toxoplasma gondii. *J. Cell Sci.* **108 (Pt 4)**, 1669–1677 (1995).
32. Lopez, J. *et al.* Intravacuolar Membranes Regulate CD8 T Cell Recognition of Membrane-Bound Toxoplasma gondii Protective Antigen. *Cell Rep.* **13**, 2273–2286 (2015).
33. Coppens, I. *et al.* Toxoplasma gondii sequesters lysosomes from mammalian hosts in the vacuolar space. *Cell* **125**, 261–274 (2006).
34. Romano, J. D., Sonda, S., Bergbower, E., Smith, M. E. & Coppens, I. Toxoplasma gondii salvages sphingolipids from the host Golgi through the rerouting of selected

Rab vesicles to the parasitophorous vacuole. *Mol. Biol. Cell* **24**, 1974–1995 (2013).

35. Karsten, V. *et al.* The protozoan parasite Toxoplasma gondii targets proteins to dense granules and the vacuolar space using both conserved and unusual mechanisms. *J. Cell Biol.* **141**, 1323–1333 (1998).
36. Cesbron-Delauw, M. F. Dense-granule organelles of Toxoplasma gondii: their role in the host-parasite relationship. *Parasitol. Today* **10**, 293–296 (1994).
37. Frénal, K. *et al.* Myosin-dependent cell-cell communication controls synchronicity of division in acute and chronic stages of Toxoplasma gondii. *Nat. Commun.* **8**, 15710 (2017).
38. Hu, K. *et al.* Daughter cell assembly in the protozoan parasite Toxoplasma gondii. *Mol. Biol. Cell* **13**, 593–606 (2002).
39. Moudy, R., Manning, T. J. & Beckers, C. J. The Loss of Cytoplasmic Potassium upon Host Cell Breakdown Triggers Egress of Toxoplasma gondii*. *J. Biol. Chem.* **276**, 41492–41501 (2001).
40. Bisio, H., Lunghi, M., Brochet, M. & Soldati-Favre, D. Phosphatidic acid governs natural egress in Toxoplasma gondii via a guanylate cyclase receptor platform. *Nat Microbiol* **4**, 420–428 (2019).
41. Arrizabalaga, G. & Boothroyd, J. C. Role of calcium during Toxoplasma gondii invasion and egress. *Int. J. Parasitol.* **34**, 361–368 (2004).
42. Brown, K. M. & Sibley, L. D. Essential cGMP Signaling in Toxoplasma Is Initiated by a Hybrid P-Type ATPase-Guanylate Cyclase. *Cell Host Microbe* **24**, 804–816.e6 (2018).
43. Yang, L. *et al.* An apically located hybrid guanylate cyclase-ATPase is critical for the initiation of Ca2+ signaling and motility in Toxoplasma gondii. *J. Biol. Chem.* **294**, 8959–8972 (2019).
44. Lourido, S., Tang, K. & Sibley, L. D. Distinct signalling pathways control Toxoplasma egress and host-cell invasion. *EMBO J.* **31**, 4524–4534 (2012).
45. Howard, B. L. *et al.* Identification of potent phosphodiesterase inhibitors that demonstrate cyclic nucleotide-dependent functions in apicomplexan parasites. *ACS Chem. Biol.* **10**, 1145–1154 (2015).

46. Brown, K. M., Long, S. & David Sibley, L. Plasma Membrane Association by N-Acylation Governs PKG Function in Toxoplasma gondii. *MBio* **8**, (2017).
47. Brochet, M. *et al.* Phosphoinositide metabolism links cGMP-dependent protein kinase G to essential Ca^{2+} signals at key decision points in the life cycle of malaria parasites. *PLoS Biol.* **12**, e1001806 (2014).
48. Fang, J., Marchesini, N. & Moreno, S. N. J. A Toxoplasma gondii phosphoinositide phospholipase C (TgPI-PLC) with high affinity for phosphatidylinositol. *Biochem. J* **394**, 417–425 (2006).
49. Bullen, H. E. *et al.* Phosphatidic Acid-Mediated Signaling Regulates Microneme Secretion in Toxoplasma. *Cell Host Microbe* **19**, 349–360 (2016).
50. Darvill, N. *et al.* Structural Basis of Phosphatidic Acid Sensing by APH in Apicomplexan Parasites. *Structure* **26**, 1059–1071.e6 (2018).
51. Taylor, C. W. & Tovey, S. C. IP(3) receptors: toward understanding their activation. *Cold Spring Harb. Perspect. Biol.* **2**, a004010 (2010).
52. Seo, M.-D., Enomoto, M., Ishiyama, N., Stathopulos, P. B. & Ikura, M. Structural insights into endoplasmic reticulum stored calcium regulation by inositol 1,4,5-trisphosphate and ryanodine receptors. *Biochim. Biophys. Acta* **1853**, 1980–1991 (2015).
53. Carruthers, V. B., Moreno, S. N. & Sibley, L. D. Ethanol and acetaldehyde elevate intracellular [Ca2+] and stimulate microneme discharge in Toxoplasma gondii. *Biochem. J* **342 (Pt 2)**, 379–386 (1999).
54. Chini, E. N., Nagamune, K., Wetzel, D. M. & Sibley, L. D. Evidence that the cADPR signalling pathway controls calcium-mediated microneme secretion in Toxoplasma gondii. *Biochem. J* **389**, 269–277 (2005).
55. Alves, E., Bartlett, P. J., Garcia, C. R. S. & Thomas, A. P. Melatonin and IP3-induced Ca2+ release from intracellular stores in the malaria parasite Plasmodium falciparum within infected red blood cells. *J. Biol. Chem.* **286**, 5905–5912 (2011).
56. Lovett, J. L. & Sibley, L. D. Intracellular calcium stores in Toxoplasma gondii govern invasion of host cells. *J. Cell Sci.* **116**, 3009–3016 (2003).
57. Pace, D. A., McKnight, C. A., Liu, J., Jimenez, V. & Moreno, S. N. J. Calcium entry

in Toxoplasma gondii and its enhancing effect of invasion-linked traits. *J. Biol. Chem.* **289**, 19637–19647 (2014).

58. McCoy, J. M., Whitehead, L., van Dooren, G. G. & Tonkin, C. J. TgCDPK3 Regulates Calcium-Dependent Egress of Toxoplasma gondii from Host Cells. *PLoS Pathog.* **8**, e1003066 (2012).
59. Lourido, S. *et al.* Calcium-dependent protein kinase 1 is an essential regulator of exocytosis in Toxoplasma. *Nature* **465**, 359–362 (2010).
60. Carruthers, V. B., Giddings, O. K. & Sibley, L. D. Secretion of micronemal proteins is associated with toxoplasma invasion of host cells. *Cell. Microbiol.* **1**, 225–235 (1999).
61. Long, S. *et al.* Calmodulin-like proteins localized to the conoid regulate motility and cell invasion by Toxoplasma gondii. *PLoS Pathog.* **13**, e1006379 (2017).
62. Meissner, M., Schlüter, D. & Soldati, D. Role of Toxoplasma gondii myosin A in powering parasite gliding and host cell invasion. *Science* **298**, 837–840 (2002).
63. Graindorge, A. *et al.* The Conoid Associated Motor MyoH Is Indispensable for Toxoplasma gondii Entry and Exit from Host Cells. *PLoS Pathog.* **12**, e1005388 (2016).
64. Friedrich, R., Yeheskel, A. & Ashery, U. DOC2B, C2 domains, and calcium: A tale of intricate interactions. *Mol. Neurobiol.* **41**, 42–51 (2010).
65. Farrell, A. *et al.* A DOC2 protein identified by mutational profiling is essential for apicomplexan parasite exocytosis. *Science* **335**, 218–221 (2012).
66. Coleman, B. I. *et al.* A Member of the Ferlin Calcium Sensor Family Is Essential for Toxoplasma gondii Rhoptry Secretion. *MBio* **9**, (2018).
67. Aquilini, E. *et al.* An Alveolata secretory machinery adapted to parasite host cell invasion. *Nat Microbiol* **6**, 425–434 (2021).
68. Sparvoli, D. *et al.* An apical membrane complex controls rhoptry exocytosis and invasion in Toxoplasma. *bioRxiv* 2022.02.25.481937 (2022) doi:10.1101/2022.02.25.481937.
69. Cerutti, A., Blanchard, N. & Besteiro, S. The Bradyzoite: A Key Developmental Stage for the Persistence and Pathogenesis of Toxoplasmosis. *Pathogens* **9**,

(2020).

70. Waldman, B. S. *et al.* Identification of a Master Regulator of Differentiation in Toxoplasma. *Cell* **180**, 359–372.e16 (2020).
71. Jeffers, V., Tampaki, Z., Kim, K. & Sullivan, W. J., Jr. A latent ability to persist: differentiation in Toxoplasma gondii. *Cell. Mol. Life Sci.* **75**, 2355–2373 (2018).
72. Cabrera, D. G. *et al.* Plasmodial Kinase Inhibitors: License to Cure? *J. Med. Chem.* **61**, 8061–8077 (2018).
73. Sauvey, C., Ehrenkaufer, G., Shi, D., Debnath, A. & Abagyan, R. Antineoplastic kinase inhibitors: A new class of potent anti-amoebic compounds. *PLoS Negl. Trop. Dis.* **15**, e0008425 (2021).
74. Merritt, C., Silva, L. E., Tanner, A. L., Stuart, K. & Pollastri, M. P. Kinases as druggable targets in trypanosomatid protozoan parasites. *Chem. Rev.* **114**, 11280–11304 (2014).
75. Hanks, S. K. & Hunter, T. Protein kinases 6. The eukaryotic protein kinase superfamily: kinase (catalytic) domain structure and classification. *FASEB J.* **9**, 576–596 (1995).
76. Zheng, J. *et al.* Crystal structure of the catalytic subunit of cAMP-dependent protein kinase complexed with MgATP and peptide inhibitor. *Biochemistry* **32**, 2154–2161 (1993).
77. Knighton, D. R. *et al.* Crystal structure of the catalytic subunit of cyclic adenosine monophosphate-dependent protein kinase. *Science* vol. 253 407–414 (1991).
78. Knighton, D. R. *et al.* Structure of a peptide inhibitor bound to the catalytic subunit of cyclic adenosine monophosphate-dependent protein kinase. *Science* **253**, 414–420 (1991).
79. Bossemeyer, D., Engh, R. A., Kinzel, V., Ponstingl, H. & Huber, R. Phosphotransferase and substrate binding mechanism of the cAMP-dependent protein kinase catalytic subunit from porcine heart as deduced from the 2.0 A structure of the complex with Mn2+ adenylyl imidodiphosphate and inhibitor peptide PKI(5-24). *EMBO J.* **12**, 849–859 (1993).
80. Bose, R., Holbert, M. A., Pickin, K. A. & Cole, P. A. Protein tyrosine kinase-

substrate interactions. *Curr. Opin. Struct. Biol.* **16**, 668–675 (2006).

81. Goldsmith, E. J., Akella, R., Min, X., Zhou, T. & Humphreys, J. M. Substrate and docking interactions in serine/threonine protein kinases. *Chem. Rev.* **107**, 5065–5081 (2007).
82. Bardwell, L. Mechanisms of MAPK signalling specificity. *Biochem. Soc. Trans.* **34**, 837–841 (2006).
83. Biondi, R. M., Kieloch, A., Currie, R. A., Deak, M. & Alessi, D. R. The PIF-binding pocket in PDK1 is essential for activation of S6K and SGK, but not PKB. *EMBO J.* **20**, 4380–4390 (2001).
84. Schechtman, D. & Mochly-Rosen, D. Adaptor proteins in protein kinase C-mediated signal transduction. *Oncogene* **20**, 6339–6347 (2001).
85. Taylor, S. S. & Kornev, A. P. Protein kinases: evolution of dynamic regulatory proteins. *Trends Biochem. Sci.* **36**, 65–77 (2011).
86. Johnson, L. N., Noble, M. E. & Owen, D. J. Active and inactive protein kinases: structural basis for regulation. *Cell* **85**, 149–158 (1996).
87. Mora, A., Komander, D., van Aalten, D. M. F. & Alessi, D. R. PDK1, the master regulator of AGC kinase signal transduction. *Semin. Cell Dev. Biol.* **15**, 161–170 (2004).
88. Wick, M. J. *et al.* Mouse 3-phosphoinositide-dependent protein kinase-1 undergoes dimerization and trans-phosphorylation in the activation loop. *J. Biol. Chem.* **278**, 42913–42919 (2003).
89. Francis, S. H., Poteet-Smith, C., Busch, J. L., Richie-Jannetta, R. & Corbin, J. D. Mechanisms of autoinhibition in cyclic nucleotide-dependent protein kinases. *Front. Biosci.* **7**, d580–92 (2002).
90. Ingram, J. R. *et al.* Allosteric activation of apicomplexan calcium-dependent protein kinases. *Proc. Natl. Acad. Sci. U. S. A.* **112**, E4975–84 (2015).
91. Currie, R. A. *et al.* Role of phosphatidylinositol 3,4,5-trisphosphate in regulating the activity and localization of 3-phosphoinositide-dependent protein kinase-1. *Biochem. J* **337 (Pt 3)**, 575–583 (1999).
92. Peixoto, L. *et al.* Integrative genomic approaches highlight a family of parasite-

specific kinases that regulate host responses. *Cell Host Microbe* **8**, 208–218 (2010).

93. Martin, D. M. A., Miranda-Saavedra, D. & Barton, G. J. Kinomer v. 1.0: a database of systematically classified eukaryotic protein kinases. *Nucleic Acids Res.* **37**, D244–50 (2009).
94. Talevich, E., Mirza, A. & Kannan, N. Structural and evolutionary divergence of eukaryotic protein kinases in Apicomplexa. *BMC Evol. Biol.* **11**, 321 (2011).
95. Gaji, R. Y., Sharp, A. K. & Brown, A. M. Protein kinases in Toxoplasma gondii. *Int. J. Parasitol.* **51**, 415–429 (2021).
96. Sidik, S. M. *et al.* Using a Genetically Encoded Sensor to Identify Inhibitors of Toxoplasma gondii Ca2+ Signaling. *J. Biol. Chem.* **291**, 9566–9580 (2016).
97. Wiersma, H. I. *et al.* A role for coccidian cGMP-dependent protein kinase in motility and invasion. *Int. J. Parasitol.* **34**, 369–380 (2004).
98. Brown, K. M., Lourido, S. & Sibley, L. D. Serum Albumin Stimulates Protein Kinase G-dependent Microneme Secretion in Toxoplasma gondii. *J. Biol. Chem.* **291**, 9554–9565 (2016).
99. Jia, Y. *et al.* Crosstalk between PKA and PKG controls pH-dependent host cell egress of Toxoplasma gondii. *EMBO J.* **36**, 3250–3267 (2017).
100. Uboldi, A. D. *et al.* Protein kinase A negatively regulates Ca2+ signalling in Toxoplasma gondii. *PLoS Biol.* **16**, e2005642 (2018).
101. Sugi, T. *et al.* Toxoplasma gondii Cyclic AMP-Dependent Protein Kinase Subunit 3 Is Involved in the Switch from Tachyzoite to Bradyzoite Development. *MBio* **7**, (2016).
102. Billker, O., Lourido, S. & Sibley, L. D. Calcium-dependent signaling and kinases in apicomplexan parasites. *Cell Host Microbe* **5**, 612–622 (2009).
103. Green, J. L. *et al.* The motor complex of Plasmodium falciparum: phosphorylation by a calcium-dependent protein kinase. *J. Biol. Chem.* **283**, 30980–30989 (2008).
104. Bansal, A. *et al.* Characterization of Plasmodium falciparum calcium-dependent protein kinase 1 (PfCDPK1) and its role in microneme secretion during erythrocyte invasion. *J. Biol. Chem.* **288**, 1590–1602 (2013).

105. Kumar, S. *et al.* Plasmodium falciparum Calcium-Dependent Protein Kinase 4 is Critical for Male Gametogenesis and Transmission to the Mosquito Vector. *MBio* **12**, e0257521 (2021).
106. Fang, H. *et al.* Epistasis studies reveal redundancy among calcium-dependent protein kinases in motility and invasion of malaria parasites. *Nat. Commun.* **9**, 4248 (2018).
107. Beraki, T. *et al.* Divergent kinase regulates membrane ultrastructure of the Toxoplasma parasitophorous vacuole. *Proc. Natl. Acad. Sci. U. S. A.* **116**, 6361–6370 (2019).
108. Taylor, S. *et al.* A secreted serine-threonine kinase determines virulence in the eukaryotic pathogen Toxoplasma gondii. *Science* **314**, 1776–1780 (2006).
109. Fox, B. A. *et al.* The Toxoplasma gondii Rhoptry Kinome Is Essential for Chronic Infection. *MBio* **7**, (2016).
110. Fleckenstein, M. C. *et al.* A Toxoplasma gondii pseudokinase inhibits host IRG resistance proteins. *PLoS Biol.* **10**, e1001358 (2012).
111. Niedelman, W. *et al.* The rhoptry proteins ROP18 and ROP5 mediate Toxoplasma gondii evasion of the murine, but not the human, interferon-gamma response. *PLoS Pathog.* **8**, e1002784 (2012).
112. Saeij, J. P. J. *et al.* Toxoplasma co-opts host gene expression by injection of a polymorphic kinase homologue. *Nature* **445**, 324–327 (2007).
113. Ong, Y.-C., Reese, M. L. & Boothroyd, J. C. Toxoplasma Rhoptry Protein 16 (ROP16) Subverts Host Function by Direct Tyrosine Phosphorylation of STAT6*. *J. Biol. Chem.* **285**, 28731–28740 (2010).
114. Yamamoto, M. *et al.* A single polymorphic amino acid on Toxoplasma gondii kinase ROP16 determines the direct and strain-specific activation of Stat3. *J. Exp. Med.* **206**, 2747–2760 (2009).
115. Alvarez, C. A. & Suvorova, E. S. Checkpoints of apicomplexan cell division identified in Toxoplasma gondii. *PLoS Pathog.* **13**, e1006483 (2017).
116. Suvorova, E. S., Francia, M., Striepen, B. & White, M. W. A novel bipartite centrosome coordinates the apicomplexan cell cycle. *PLoS Biol.* **13**, e1002093

(2015).

117. Berry, L. *et al.* The conserved apicomplexan Aurora kinase TgArk3 is involved in endodyogeny, duplication rate and parasite virulence. *Cell. Microbiol.* **18**, 1106–1120 (2016).
118. Naumov, A. *et al.* The Toxoplasma Centrocone Houses Cell Cycle Regulatory Factors. *MBio* **8**, (2017).
119. Pfefferkorn, E. R. & Pfefferkorn, L. C. Toxoplasma gondii: isolation and preliminary characterization of temperature-sensitive mutants. *Exp. Parasitol.* **39**, 365–376 (1976).
120. Pfefferkorn, E. R. & Pfefferkorn, L. C. Toxoplasma gondii: characterization of a mutant resistant to 5-fluorodeoxyuridine. *Exp. Parasitol.* **42**, 44–55 (1977).
121. Pfefferkorn, E. R. & Pfefferkorn, L. C. Arabinosyl nucleosides inhibit Toxoplasma gondii and allow the selection of resistant mutants. *J. Parasitol.* **62**, 993–999 (1976).
122. Pfefferkorn, L. C. & Pfefferkorn, E. R. Toxoplasma gondii: genetic recombination between drug resistant mutants. *Exp. Parasitol.* **50**, 305–316 (1980).
123. Pfefferkorn, E. R. & Kasper, L. H. Toxoplasma gondii: genetic crosses reveal phenotypic suppression of hydroxyurea resistance by fluorodeoxyuridine resistance. *Exp. Parasitol.* **55**, 207–218 (1983).
124. Sibley, L. D., LeBlanc, A. J., Pfefferkorn, E. R. & Boothroyd, J. C. Generation of a restriction fragment length polymorphism linkage map for Toxoplasma gondii. *Genetics* **132**, 1003–1015 (1992).
125. Su, C., Howe, D. K., Dubey, J. P., Ajioka, J. W. & Sibley, L. D. Identification of quantitative trait loci controlling acute virulence in Toxoplasma gondii. *Proc. Natl. Acad. Sci. U. S. A.* **99**, 10753–10758 (2002).
126. Donald, R. G. & Roos, D. S. Stable molecular transformation of Toxoplasma gondii: a selectable dihydrofolate reductase-thymidylate synthase marker based on drug-resistance mutations in malaria. *Proc. Natl. Acad. Sci. U. S. A.* **90**, 11703–11707 (1993).
127. Soldati, D. & Boothroyd, J. C. Transient transfection and expression in the obligate

intracellular parasite Toxoplasma gondii. *Science* **260**, 349–352 (1993).

128. Kim, K., Soldati, D. & Boothroyd, J. C. Gene replacement in Toxoplasma gondii with chloramphenicol acetyltransferase as selectable marker. *Science* **262**, 911–914 (1993).

129. Huynh, M.-H. & Carruthers, V. B. Tagging of endogenous genes in a Toxoplasma gondii strain lacking Ku80. *Eukaryot. Cell* **8**, 530–539 (2009).

130. Fox, B. A., Ristuccia, J. G., Gigley, J. P. & Bzik, D. J. Efficient gene replacements in Toxoplasma gondii strains deficient for nonhomologous end joining. *Eukaryot. Cell* **8**, 520–529 (2009).

131. Sidik, S. M., Hackett, C. G., Tran, F., Westwood, N. J. & Lourido, S. Efficient genome engineering of Toxoplasma gondii using CRISPR/Cas9. *PLoS One* **9**, e100450 (2014).

132. Shen, B., Brown, K. M., Lee, T. D. & Sibley, L. D. Efficient gene disruption in diverse strains of Toxoplasma gondii using CRISPR/CAS9. *MBio* **5**, e01114–14 (2014).

133. Meissner, M., Brecht, S., Bujard, H. & Soldati, D. Modulation of myosin A expression by a newly established tetracycline repressor-based inducible system in Toxoplasma gondii. *Nucleic Acids Res.* **29**, E115 (2001).

134. van Poppel, N. F. J., Welagen, J., Duisters, R. F. J. J., Vermeulen, A. N. & Schaap, D. Tight control of transcription in Toxoplasma gondii using an alternative tet repressor. *Int. J. Parasitol.* **36**, 443–452 (2006).

135. Andenmatten, N. *et al.* Conditional genome engineering in Toxoplasma gondii uncovers alternative invasion mechanisms. *Nat. Methods* **10**, 125–127 (2013).

136. Pieperhoff, M. S. *et al.* Conditional U1 Gene Silencing in Toxoplasma gondii. *PLoS One* **10**, e0130356 (2015).

137. Hunt, A. *et al.* Differential requirements for cyclase-associated protein (CAP) in actin-dependent processes of Toxoplasma gondii. *Elife* **8**, (2019).

138. Nishimura, K., Fukagawa, T., Takisawa, H., Kakimoto, T. & Kanemaki, M. An auxin-based degron system for the rapid depletion of proteins in nonplant cells. *Nat. Methods* **6**, 917–922 (2009).

139. Gubbels, M.-J. *et al.* Forward genetic analysis of the apicomplexan cell division cycle in Toxoplasma gondii. *PLoS Pathog.* **4**, e36 (2008).
140. Sidik, S. M. *et al.* A Genome-wide CRISPR Screen in Toxoplasma Identifies Essential Apicomplexan Genes. *Cell* **166**, 1423–1435.e12 (2016).
141. Bushell, E. *et al.* Functional Profiling of a Plasmodium Genome Reveals an Abundance of Essential Genes. *Cell* **170**, 260–272.e8 (2017).
142. Zhang, M. *et al.* Uncovering the essential genes of the human malaria parasite Plasmodium falciparum by saturation mutagenesis. *Science* **360**, (2018).
143. Young, J. *et al.* A CRISPR platform for targeted in vivo screens identifies Toxoplasma gondii virulence factors in mice. *Nat. Commun.* **10**, 3963 (2019).
144. Sangaré, L. O. *et al.* In Vivo CRISPR Screen Identifies TgWIP as a Toxoplasma Modulator of Dendritic Cell Migration. *Cell Host Microbe* **26**, 478–492.e8 (2019).
145. Harding, C. R. *et al.* Genetic screens reveal a central role for heme metabolism in artemisinin susceptibility. *Nat. Commun.* **11**, 4813 (2020).
146. Hamilton, W. L. *et al.* Extreme mutation bias and high AT content in Plasmodium falciparum. *Nucleic Acids Res.* **45**, 1889–1901 (2017).
147. Krogan, N. J. *et al.* Global landscape of protein complexes in the yeast Saccharomyces cerevisiae. *Nature* **440**, 637–643 (2006).
148. Huh, W.-K. *et al.* Global analysis of protein localization in budding yeast. *Nature* **425**, 686–691 (2003).
149. Weill, U. *et al.* Genome-wide SWAp-Tag yeast libraries for proteome exploration. *Nat. Methods* **15**, 617–622 (2018).
150. Dean, S., Sunter, J. D. & Wheeler, R. J. TrypTag.org: A Trypanosome Genome-wide Protein Localisation Resource. *Trends Parasitol.* **33**, 80–82 (2017).
151. Leonetti, M. D., Sekine, S., Kamiyama, D., Weissman, J. S. & Huang, B. A scalable strategy for high-throughput GFP tagging of endogenous human proteins. *Proc. Natl. Acad. Sci. U. S. A.* **113**, E3501–8 (2016).
152. Cho, N. H. *et al.* OpenCell: proteome-scale endogenous tagging enables the cartography of human cellular organization. *bioRxiv* 2021.03.29.437450 (2021) doi:10.1101/2021.03.29.437450.

153. Sathyan, K. M. *et al.* An improved auxin-inducible degron system preserves native protein levels and enables rapid and specific protein depletion. *Genes Dev.* **33**, 1441–1455 (2019).
154. Long, S., Anthony, B., Drewry, L. L. & Sibley, L. D. A conserved ankyrin repeat-containing protein regulates conoid stability, motility and cell invasion in Toxoplasma gondii. *Nat. Commun.* **8**, 2236 (2017).
155. Brown, K. M., Long, S. & Sibley, L. D. Conditional Knockdown of Proteins Using Auxin-inducible Degron (AID) Fusions in Toxoplasma gondii. *Bio Protoc* **8**, (2018).
156. Harding, C. R. *et al.* Gliding Associated Proteins Play Essential Roles during the Formation of the Inner Membrane Complex of Toxoplasma gondii. *PLoS Pathog.* **12**, e1005403 (2016).
157. Barylyuk, K. *et al.* A Comprehensive Subcellular Atlas of the Toxoplasma Proteome via hyperLOPIT Provides Spatial Context for Protein Functions. *Cell Host Microbe* **28**, 752–766.e9 (2020).
158. Varberg, J. M., Coppens, I., Arrizabalaga, G. & Gaji, R. Y. TgTKL1 Is a Unique Plant-Like Nuclear Kinase That Plays an Essential Role in Acute Toxoplasmosis. *MBio* **9**, (2018).
159. Silljé, H. H., Takahashi, K., Tanaka, K., Van Houwe, G. & Nigg, E. A. Mammalian homologues of the plant Tousled gene code for cell-cycle-regulated kinases with maximal activities linked to ongoing DNA replication. *EMBO J.* **18**, 5691–5702 (1999).
160. Pilyugin, M., Demmers, J., Verrijzer, C. P., Karch, F. & Moshkin, Y. M. Phosphorylation-mediated control of histone chaperone ASF1 levels by Tousled-like kinases. *PLoS One* **4**, e8328 (2009).
161. Silljé, H. H. & Nigg, E. A. Identification of human Asf1 chromatin assembly factors as substrates of Tousled-like kinases. *Curr. Biol.* **11**, 1068–1073 (2001).
162. Eckert, D. *et al.* Prp4 Kinase Grants the License to Splice: Control of Weak Splice Sites during Spliceosome Activation. *PLoS Genet.* **12**, e1005768 (2016).
163. Chen, C.-T. & Gubbels, M.-J. The Toxoplasma gondii centrosome is the platform for internal daughter budding as revealed by a Nek1 kinase mutant. *J. Cell Sci.*

126, 3344–3355 (2013).

164. Hu, X., O'Shaughnessy, W. J., Beraki, T. G. & Reese, M. L. Loss of the Conserved Alveolate Kinase MAPK2 Decouples Toxoplasma Cell Growth from Cell Division. *MBio* **11**, (2020).
165. Martín Moyano, P., Němec, V. & Paruch, K. Cdc-Like Kinases (CLKs): Biology, Chemical Probes, and Therapeutic Potential. *Int. J. Mol. Sci.* **21**, (2020).
166. Berto, G., Ferreira-Cerca, S. & De Wulf, P. The Rio1 protein kinases/ATPases: conserved regulators of growth, division, and genomic stability. *Curr. Genet.* **65**, 457–466 (2019).
167. Mallari, J. P., Oksman, A., Vaupel, B. & Goldberg, D. E. Kinase-associated endopeptidase 1 (Kae1) participates in an atypical ribosome-associated complex in the apicoplast of Plasmodium falciparum. *J. Biol. Chem.* **289**, 30025–30039 (2014).
168. Sampels, V. *et al.* Conditional mutagenesis of a novel choline kinase demonstrates plasticity of phosphatidylcholine biogenesis and gene expression in Toxoplasma gondii. *J. Biol. Chem.* **287**, 16289–16299 (2012).
169. Doench, J. G. *et al.* Optimized sgRNA design to maximize activity and minimize off-target effects of CRISPR-Cas9. *Nat. Biotechnol.* **34**, 184–191 (2016).
170. McInnes, L., Healy, J. & Melville, J. UMAP: Uniform Manifold Approximation and Projection for Dimension Reduction. *arXiv* 1–51 (2018).
171. Hartigan, J. A. & Wong, M. A. Algorithm AS 136: A K-means clustering algorithm. *J. R. Stat. Soc. Ser. C Appl. Stat.* **28**, 100 (1979).
172. Donald, R. G. K. *et al.* Toxoplasma gondii cyclic GMP-dependent kinase: chemotherapeutic targeting of an essential parasite protein kinase. *Eukaryot. Cell* **1**, 317–328 (2002).
173. Katso, R. *et al.* Cellular function of phosphoinositide 3-kinases: implications for development, homeostasis, and cancer. *Annu. Rev. Cell Dev. Biol.* **17**, 615–675 (2001).
174. Balla, A. & Balla, T. Phosphatidylinositol 4-kinases: old enzymes with emerging functions. *Trends Cell Biol.* **16**, 351–361 (2006).

175. Dvorin, J. D. *et al.* A plant-like kinase in Plasmodium falciparum regulates parasite egress from erythrocytes. *Science* **328**, 910–912 (2010).
176. Kato, N. *et al.* Gene expression signatures and small-molecule compounds link a protein kinase to Plasmodium falciparum motility. *Nat. Chem. Biol.* **4**, 347–356 (2008).
177. Alsford, S. *et al.* High-throughput phenotyping using parallel sequencing of RNA interference targets in the African trypanosome. *Genome Res.* **21**, 915–924 (2011).
178. Li, W. *et al.* A phenotypic screen using splitCas9 identifies essential genes required for actin regulation during host cell egress and invasion by Toxoplasma gondii. *bioRxiv* 2021.09.24.461619 (2021) doi:10.1101/2021.09.24.461619.
179. Chen, F., Mackey, A. J., Stoeckert, C. J., Jr & Roos, D. S. OrthoMCL-DB: querying a comprehensive multi-species collection of ortholog groups. *Nucleic Acids Res.* **34**, D363–8 (2006).
180. Rosenberg, A., Luth, M. R., Winzeler, E. A., Behnke, M. & Sibley, L. D. Evolution of resistance in vitro reveals mechanisms of artemisinin activity in Toxoplasma gondii. *Proc. Natl. Acad. Sci. U. S. A.* (2019) doi:10.1073/pnas.1914732116.
181. Hitz, E. *et al.* The 3-phosphoinositide-dependent protein kinase 1 is an essential upstream activator of protein kinase A in malaria parasites. *PLoS Biol.* **19**, e3001483 (2021).
182. Dittrich, A. C. N. & Devarenne, T. P. Perspectives in PDK1 evolution: insights from photosynthetic and non-photosynthetic organisms. *Plant Signal. Behav.* **7**, 642–649 (2012).
183. McRobert, L. *et al.* Gametogenesis in malaria parasites is mediated by the cGMP-dependent protein kinase. *PLoS Biol.* **6**, e139 (2008).
184. Collins, C. R. *et al.* Malaria parasite cGMP-dependent protein kinase regulates blood stage merozoite secretory organelle discharge and egress. *PLoS Pathog.* **9**, e1003344 (2013).
185. Chen, T.-W. *et al.* Ultrasensitive fluorescent proteins for imaging neuronal activity. *Nature* **499**, 295–300 (2013).
186. Tosetti, N., Dos Santos Pacheco, N., Soldati-Favre, D. & Jacot, D. Three F-actin

assembly centers regulate organelle inheritance, cell-cell communication and motility in Toxoplasma gondii. *Elife* **8**, (2019).

187. Lovett, J. L., Marchesini, N., Moreno, S. N. J. & Sibley, L. D. Toxoplasma gondii microneme secretion involves intracellular Ca(2+) release from inositol 1,4,5-triphosphate (IP(3))/ryanodine-sensitive stores. *J. Biol. Chem.* **277**, 25870–25876 (2002).
188. Bullen, H. E., Bisio, H. & Soldati-Favre, D. The triumvirate of signaling molecules controlling Toxoplasma microneme exocytosis: Cyclic GMP, calcium, and phosphatidic acid. *PLoS Pathog.* **15**, e1007670 (2019).
189. Leroux, A. E., Schulze, J. O. & Biondi, R. M. AGC kinases, mechanisms of regulation and innovative drug development. *Semin. Cancer Biol.* **48**, 1–17 (2018).
190. Paul, A. S. *et al.* Co-option of Plasmodium falciparum PP1 for egress from host erythrocytes. *Nat. Commun.* **11**, 3532 (2020).
191. Zeeshan, M. *et al.* Protein phosphatase 1 regulates atypical mitotic and meiotic division in Plasmodium sexual stages. *Commun Biol* **4**, 760 (2021).
192. Feldman, D. *et al.* Optical Pooled Screens in Human Cells. *Cell* **179**, 787–799.e17 (2019).
193. Amos, B. *et al.* VEuPathDB: the eukaryotic pathogen, vector and host bioinformatics resource center. *Nucleic Acids Res.* **50**, D898–D911 (2022).
194. Lourido, S., Jeschke, G. R., Turk, B. E. & Sibley, L. D. Exploiting the unique ATP-binding pocket of toxoplasma calcium-dependent protein kinase 1 to identify its substrates. *ACS Chem. Biol.* **8**, 1155–1162 (2013).
195. Markus, B. M., Bell, G. W., Lorenzi, H. A. & Lourido, S. Optimizing Systems for Cas9 Expression in Toxoplasma gondii. *mSphere* **4**, (2019).
196. Paquet, D. *et al.* Efficient introduction of specific homozygous and heterozygous mutations using CRISPR/Cas9. *Nature* **533**, 125–129 (2016).
197. Dewari, P. S. *et al.* An efficient and scalable pipeline for epitope tagging in mammalian stem cells using Cas9 ribonucleoprotein. *Elife* **7**, (2018).
198. Bialk, P., Rivera-Torres, N., Strouse, B. & Kmiec, E. B. Regulation of Gene Editing Activity Directed by Single-Stranded Oligonucleotides and CRISPR/Cas9 Systems.

PLoS One **10**, e0129308 (2015).

199. Liang, X., Potter, J., Kumar, S., Ravinder, N. & Chesnut, J. D. Enhanced CRISPR/Cas9-mediated precise genome editing by improved design and delivery of gRNA, Cas9 nuclease, and donor DNA. *J. Biotechnol.* **241**, 136–146 (2017).
200. Burg, J. L., Perelman, D., Kasper, L. H., Ware, P. L. & Boothroyd, J. C. Molecular analysis of the gene encoding the major surface antigen of Toxoplasma gondii. *J. Immunol.* **141**, 3584–3591 (1988).
201. Starnes, G. L., Jewett, T. J., Carruthers, V. B. & Sibley, L. D. Two separate, conserved acidic amino acid domains within the Toxoplasma gondii MIC2 cytoplasmic tail are required for parasite survival. *J. Biol. Chem.* **281**, 30745–30754 (2006).
202. Plattner, F. *et al.* Toxoplasma profilin is essential for host cell invasion and TLR11-dependent induction of an interleukin-12 response. *Cell Host Microbe* **3**, 77–87 (2008).
203. Shortt, E. & Lourido, S. Plate-Based Quantification of Stimulated Toxoplasma Egress. *Methods Mol. Biol.* **2071**, 171–186 (2020).
204. Smith, T. A., Lopez-Perez, G. S., Shortt, E. & Lourido, S. High-throughput functionalization of the Toxoplasma kinome uncovers a novel regulator of invasion and egress. *bioRxiv* 2021.09.23.461611 (2021) doi:10.1101/2021.09.23.461611.

EXTENDED DATA FIGURES

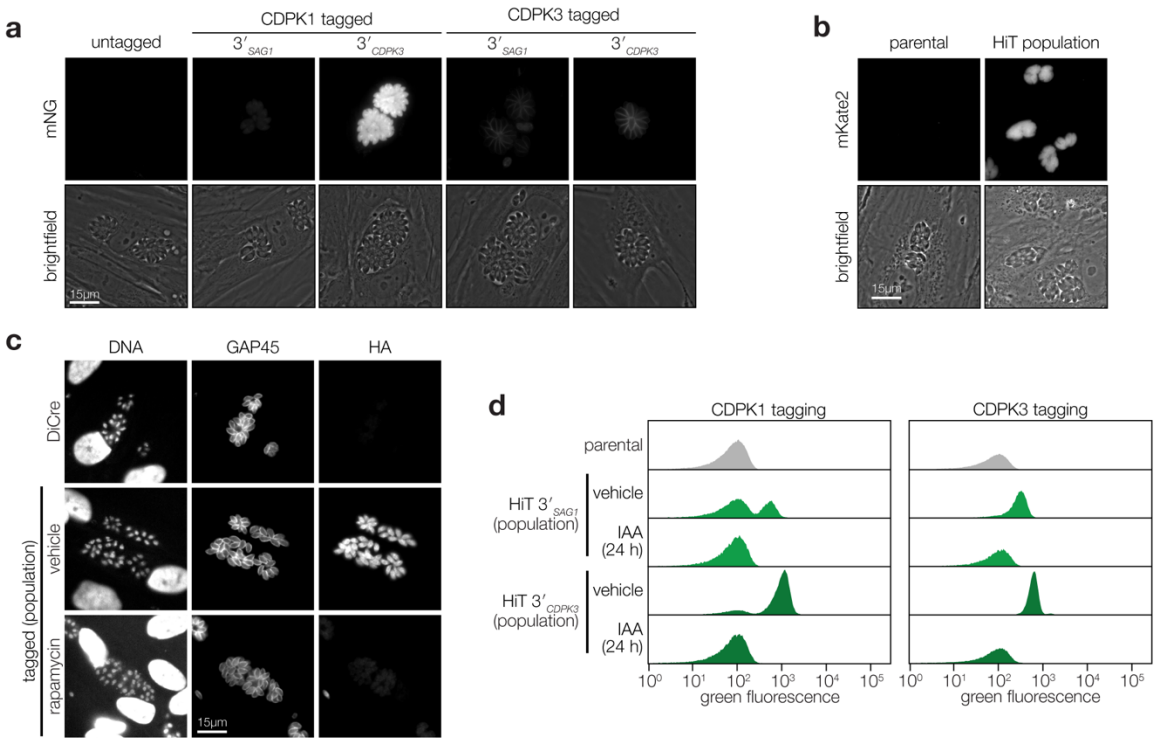

Extended Data Figure 1. Transfected populations efficiently incorporate a variety of HiT vectors. **a**, Fluorescence microscopy of the tagged populations displaying the correct localization of each kinase and expression levels consistent with flow cytometry (**Fig. 1b**). **b**, Live microscopy of V5-T2A-mKate2 HiT-tagged population (merged image in **Fig. 2d**). **c**, Immunofluorescence microscopy of population tagged with the HA-U1 HiT vector following treatment with rapamycin or vehicle control (merged image in **Fig. 2f**). **d**, Flow cytometry of parasite populations tagged with the V5-mNG-mAID HiT vector targeting *CDPK1* or *CDPK3* and treated with either IAA or vehicle control for 24 h (excerpt shown in Fig. 1l).

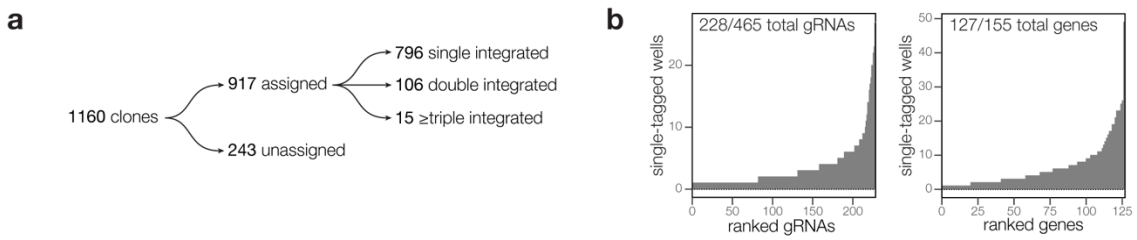

Extended Data Figure 2. Arrayed screening results. a, Results from dual-indexed sequencing of the arrayed clones. A minimum of 100 reads were required to assign a given gRNA to a particular clone. Cases where a second gRNA reached >10% the abundance of the first gRNA were classified as containing multiple integrations. **b**, Histogram showing the distribution of gRNAs and genes contained among single-integrated wells within the array. Genes and gRNAs with no representation are omitted from the plot.

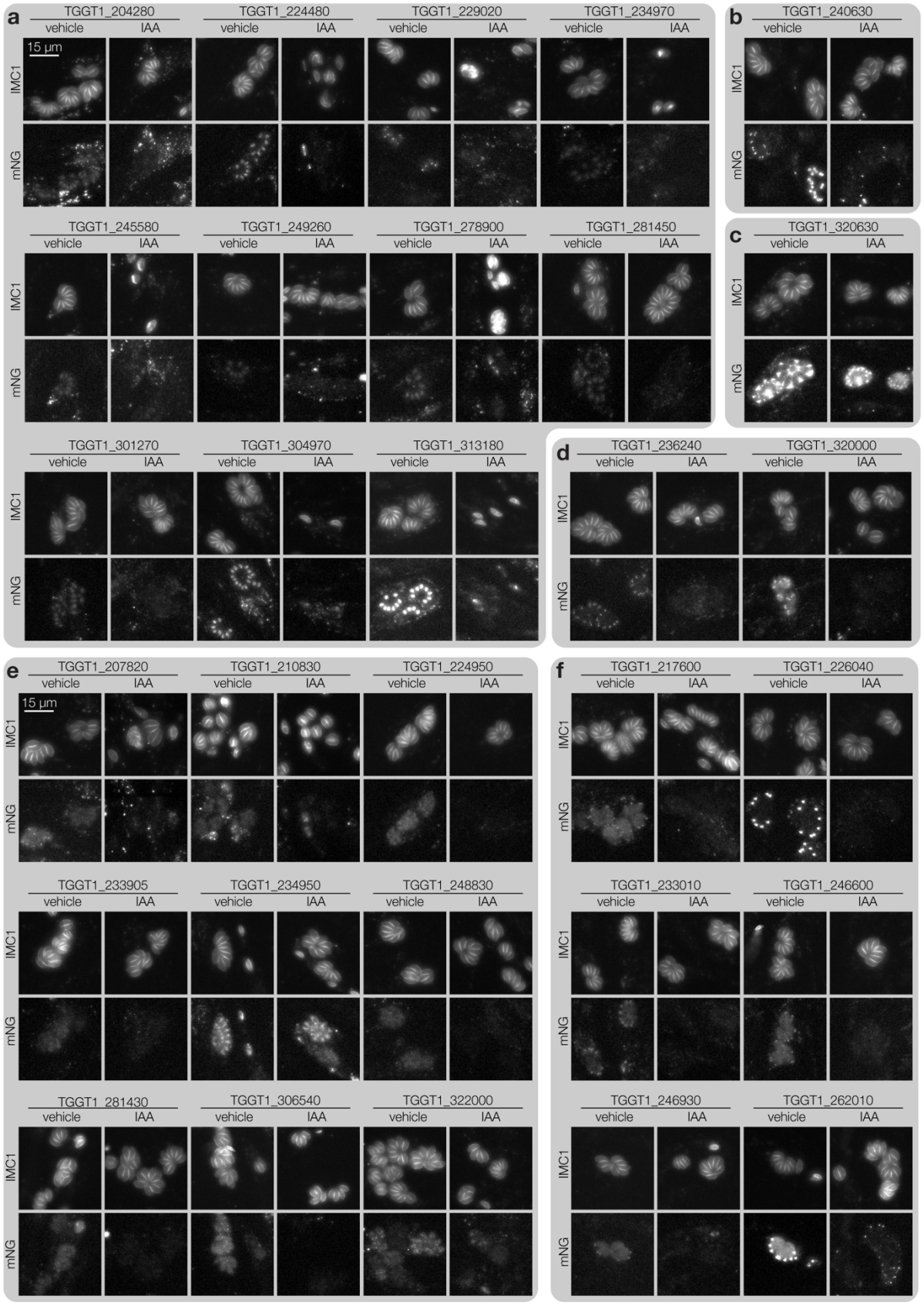
a
TGGT1_204280
TGGT1_224480
TGGT1_229020
TGGT1_234970
vehicle
IAA
15 µm
IMC1
mNG
TGGT1_245580
TGGT1_249260
TGGT1_278900
TGGT1_281450
TGGT1_301270
TGGT1_304970
TGGT1_313180
b
TGGT1_240630
c
TGGT1_320630
d
TGGT1_236240
TGGT1_320000
e
TGGT1_207820
TGGT1_210830
TGGT1_224950
TGGT1_233905
TGGT1_234950
TGGT1_248830
TGGT1_281430
TGGT1_306540
TGGT1_322000
f
TGGT1_217600
TGGT1_226040
TGGT1_233010
TGGT1_246600
TGGT1_246930
TGGT1_262010

Extended Data Figure 3. Representative images from the arrayed screen. a–f, Widefield microscopy of representative clones. Maximum intensity projections for IMC1-tdTomato and mNeonGreen-tagged targets are displayed for cultures treated with either IAA or vehicle for 24 hours. All images are displayed at the same scale. Localizations to the nucleus (**a**), daughter cell IMC (**b**), parasitophorous vacuole (**c**), perinuclear space (**d**), cytosol (**e**) or apical end (**f**) were assigned to a gene if half or more of single-integrated wells for that gene displayed consistent localizations.

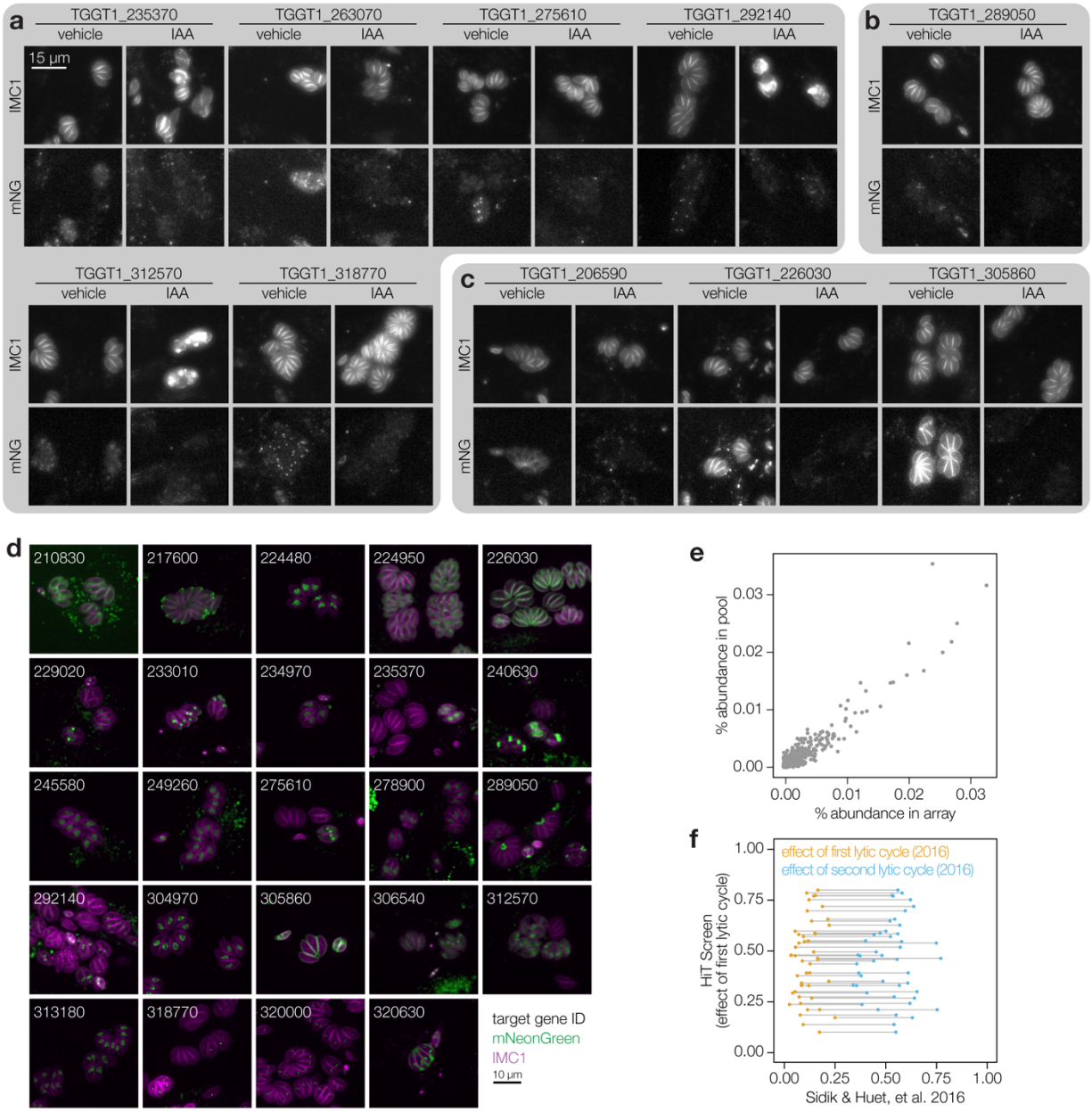

Extended Data Figure 4. Additional representative images from the arrayed screen and comparisons to the pooled results. a–c, Widefield microscopy of representative clones. Maximum intensity projections for IMC1-tdTomato and mNeonGreen-tagged targets are displayed for cultures treated with either IAA or vehicle for 24 hours. All images are displayed at the same scale. Localizations to puncta (**a**), the basal end (**b**), or peripheral structures (**c**) were assigned to a gene if half or more of single-integrated wells for that gene displayed consistent localizations. **d**, Representative confocal images of a sample of clones. mNeonGreen (green); IMC1-tdTomato (magenta). Images are maximum intensity projections. Genes are numbered based on the unique identifier from ToxoDB (e.g., TGGT1_210830, labeled 210830). **e**, Comparison of relative gRNA abundances in the array compared to the pooled population that was subcloned. Spearman correlation coefficient = 0.77. **f**, Impact of the initial lytic cycles on gRNA abundance for genes with delayed or acute loss phenotypes in the HiT screen. The effect of the first lytic cycle from the HiT screen is plotted against the effect of the first or second lytic

cycles for the genome-wide knockout screen (Sidik & Huet, et al. 2016). Genes are paired across their first and second lytic cycles within the genome-wide knockout screen.

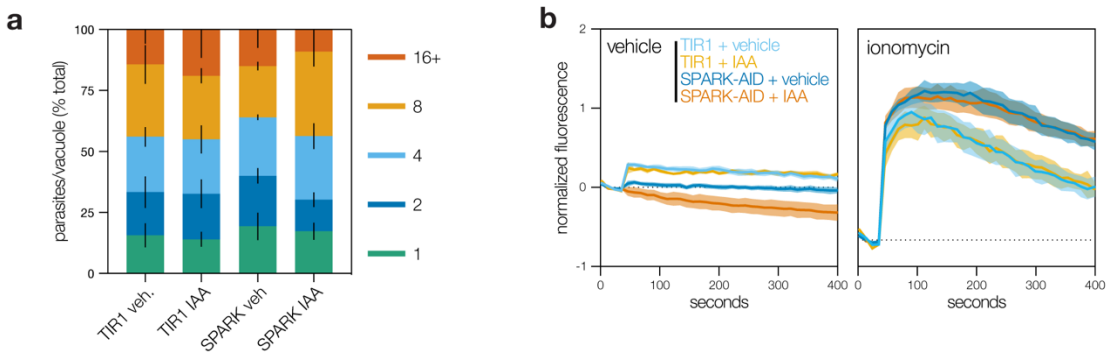

Extended Data Figure 5. Extended analysis of SPARK depletion. a, Replication assay of SPARK-AID parasites. Parasites were treated with either IAA or vehicle at 3 hours post-invasion and imaged 24 hours later. The number of parasites per vacuole were counted for 100 vacuoles per sample. Mean ± S.E. graphed for *n* = 3 biological replicates. **b**, Extracellular parasites in basal Ca^{2+} buffer stimulated with vehicle or the Ca^{2+} ionophore ionomycin, following 24 h of treatment with vehicle or IAA. Cytosolic Ca^{2+} flux was measured in bulk as GCaMP6f fluorescence normalized to the initial and maximum fluorescence following aerolysin permeabilization in 2 mM Ca^{2+}. Mean ± S.E. graphed for *n* = 3–6 biological replicates.

SUPPLEMENTARY FIGURES

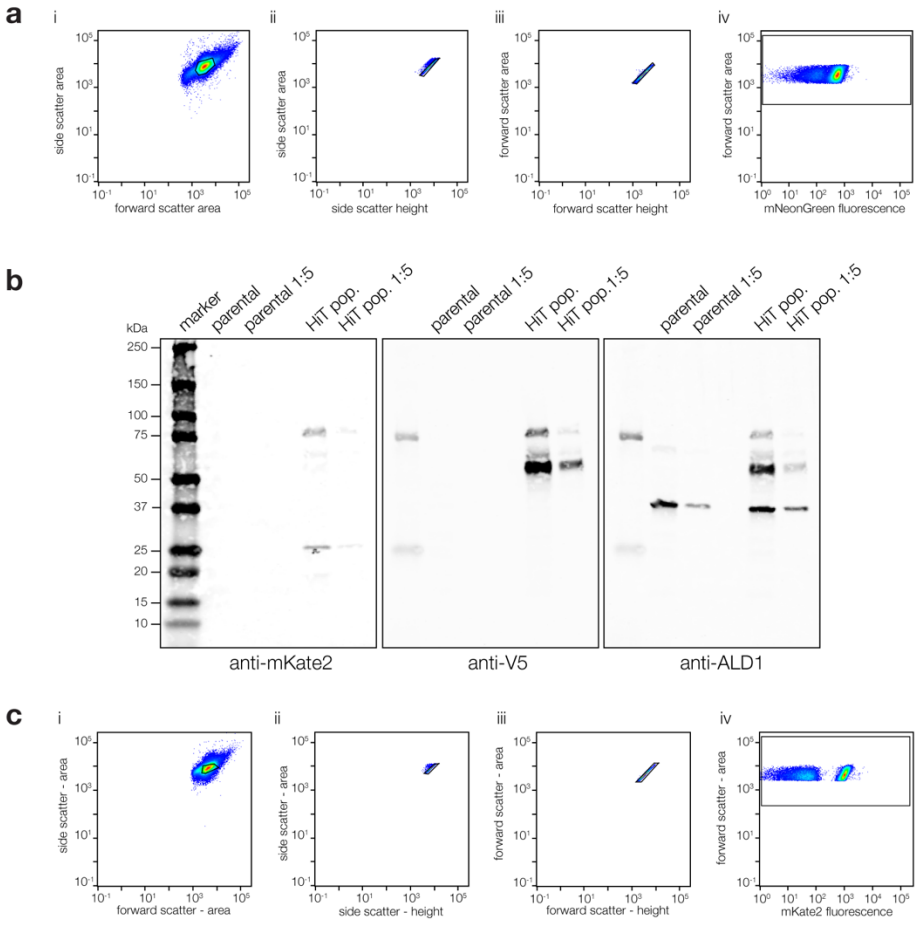

Supplementary Figure 1. Flow cytometry gating strategies and complete immunoblot of transfected HiT populations. a, Flow cytometry gating strategy for **Fig. 1b**, **Fig. 1l**, and **Extended Data Fig. 1d**. Events were subsequently gated for toxoplasma (i) and single cells (ii–iii). Events were used to create histograms of mNeonGreen fluorescence in **Fig. 1b**, **Fig. 2i**, and **Extended Data Fig. 1d** (iv). Example pseudocolor density plots are provided from the CDPK3 HiT 3′$_{CDPK3}$ population of **Fig. 1b**. **b**, Complete immunoblot from **Fig. 2c**. CDPK1-V5-T2A was detected using an anti-V5 antibody, mKate2 was detected using an anti-RFP antibody, and ALD1 was used as a loading control. **c**, Flow cytometry gating strategy for **Fig. 2b**. Events were subsequently gated for toxoplasma (i) and single cells (ii–iii). Events were used to create a histogram of mKate2 fluorescence in **Fig. 2b** (iv). Example pseudocolor density plots are provided from the CDPK1 HiT 3′$_{CDPK3}$ population of **Fig. 2b**.

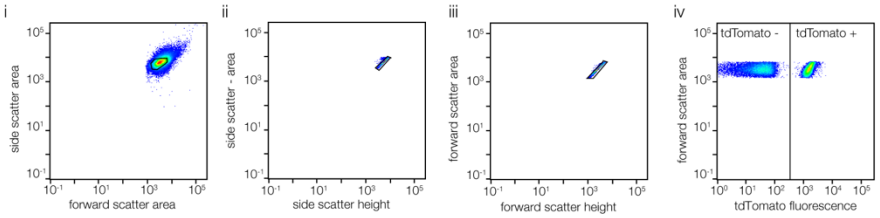

Supplementary Figure 2. Flow cytometry gating strategy of competition experiments. Flow cytometry gating strategy for **Fig. 6b**. Events were subsequently gated for toxoplasma (i) and single cells (ii–iii). Events were binned as either tdTomato positive or tdTomato negative using the TIR1 and TIR1/IMC1-tdTomato strains as references (iv). Example pseudocolor density plots are provided from the starting population of the WT sample.

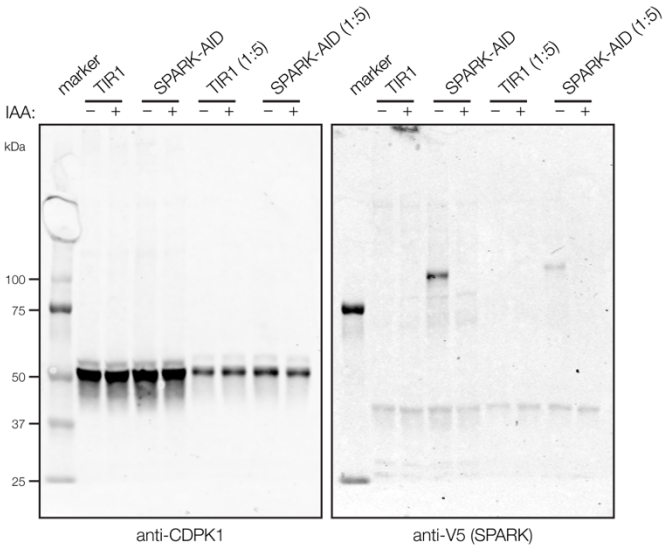

Supplementary Figure 3. Complete immunoblot of SPARK knockdown. Full immunoblot from **Fig. 7d**. SPARK-AID was detected using an anti-V5 antibody and CDPK1 was used as a loading control.